(4)

THE OHIO STATE UNIVERSITY

High Resolution Exponential Modeling of Fully Polarized Radar Returns

W.M. Steedly and R.L. Moses

The Ohio State University

ElectroScience Laboratory

Department of Electrical Engineering
Columbus, Ohio 43212

Technical Report 718048-13
Contract No. N00014-86-K-0202
November 1989

Department of the Navy
Office of Naval Research
800 North Quincy Street
Arlington, Virginia 22217-5000

NOTICES

When Government drawings, specifications, or other data are used for any purpose other than in connection with a definitely related Government procurement operation, the United States Government thereby incurs no responsibility nor any obligation whatsoever, and the fact that the Government may have formulated, furnished, or in any way supplied the said drawings, specifications, or other data, is not to be regarded by implication or otherwise as in any manner licensing the holder or any other person or corporation, or conveying any rights or permission to manufacture, use, or sell any patented invention that may in any way be related thereto.

50272-101

REPORT DOCUMENTATION PAGE	1. REPORT NO.	2.	3. Recipient's Accession No.

4. Title and Subtitle
High Resolution Exponential Modeling of Fully Polarized Radar Returns

5. Report Date
November 1989

6.

7. Author(s)
W.E. Steedly, R.L. Moses

8. Performing Org. Rept. No.
718048-13

9. Performing Organization Name and Address
The Ohio State University
ElectroScience Laboratory
1320 Kinnear Road
Columbus, OH 43212

10. Project/Task/Work Unit No.

11. Contract(C) or Grant(G) No.
(C) N00014-86-K-0202
(G)

12. Sponsoring Organization Name and Address
Office of Naval Research
Room 804, Code 1211, 800 North Quincy Street
Washington, D.C. 22217

13. Report Type/Period Covered
Technical Report

14.

15. Supplementary Notes

16. Abstract (Limit: 200 words)

This report considers a new method for modeling radar target scattering data for the purposes of automatic target recognition. The approach is to estimate a time (range) domain feature vector which describes the target. In particular, the target is characterized by a set of attributed scattering centers using the notion of a Transient Polarization Response; not only are scattering centers and their energies determined, but also their polarization effects on a circularly polarized incident wave, which are in general elliptical. An exponential model for the fully polarized radar return and an algorithm to estimate those parameters are presented. This algorithm is then applied to compact range measurements of aircraft models, and the results are presented and discussed.

17. Document Analysis a. Descriptors

b. Identifiers/Open-Ended Terms

c. COSATI Field/Group

18. Availability Statement
A. Approved for public release;
Distribution is unlimited.

19. Security Class (This Report)
Unclassified

21. No. of Pages
60

20. Security Class (This Page)
Unclassified

22. Price

(See ANSI-Z39.18) *See Instructions on Reverse* OPTIONAL FORM 272 (4-77)
Department of Commerce

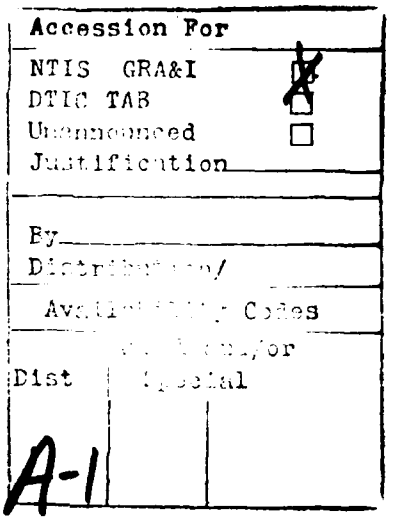

Contents

List of Figures

List of Tables

Chapter 1

Introduction

This report is concerned with processing the fully polarized radar return of a target in order to gain more information about the target. This work has application to the area of radar target identification (RTI). Presently the capabilities of most operational aircraft radar systems are limited to the detection of an aircraft and the determination of its position and velocity. It is always desirable to gain more information about unknown aircraft. One method is to identify an aircraft by detecting its jet engine modulation (JEM) line signatures; however, this technique yields information limited to engine structure. More information about the physical structure of the entire aircraft including its size, layout, and armaments is needed. To this end many ways of processing stepped frequency radar measurements have been developed [1]–[8] in order to determine physical information about the aircraft target such as overall length.

To arrive at the goal of determining such information, this report considers a method for modeling of radar target signatures from a set of full polarization stepped frequency measurements of the target. The target

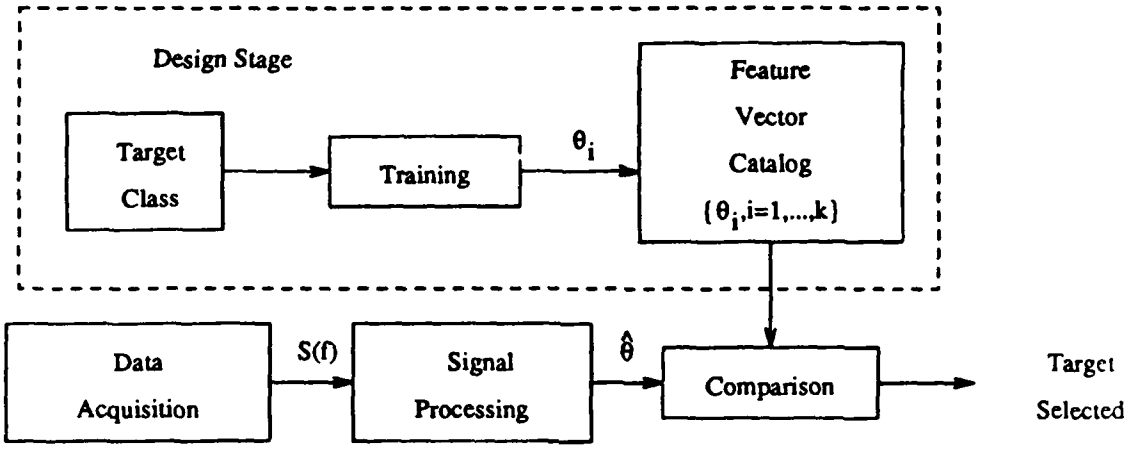

Figure 1.1: The Automatic Target Recognition Problem

signature is modeled using an exponential model, which characterizes the target as a set of attributed scattering centers. This modeling step has application in automatic target recognition (ATR).

A block diagram of an ATR system is shown in Figure 1.1. During the design stage, data from a set of known targets or target classes is used in a training step to arrive at a set of feature vectors θ_i, where each vector describes a target class. This catalog of feature vectors is stored for use in classification. In the operation stage, data of an unknown target is measured and undergoes a signal processing operation. The output of the signal processing operation is an estimated feature vector $\hat{\theta}$ of the unknown target. This estimate is compared to the catalog, and the "closest" match is found to identify the target.

The signal processing operation has a major impact on the performance of the system and is the focus of this report. One desires a feature vector $\hat{\theta}$ which is small in dimension (to keep the computational requirements of the classifier at a modest level), but at the same time has little or no information loss as compared to the original measurements. In addition, the features in $\hat{\theta}$ should be robust to effects of noise, clutter, and target orientation.

One method of ATR is to directly use the stepped frequency measurements as a feature vector, and to apply parametric or non-parametric pattern recognition techniques to this feature vector [1,3,4]. However, working directly in the frequency domain can have disadvantages. For example, in a wideband radar system, many frequencies may be used, so the length of the feature vector may be prohibitively large, making the classification procedure computationally intensive.

In this report, the approach taken is to estimate a time (range) domain feature vector which describes the target. In particular, the target is characterized by a set of scattering centers. This idea has been used for some time for single polarization measurements. The approach is to locate scattering centers either by taking the Fast Fourier Transform (FFT) of the frequency measurements and locating the peaks [2] or to use parametric models, such as autoregressive or autoregressive moving average models to parameterize the peak response profile [2,6,7]. The advantages of time domain characterizations are that the target can be modeled as a relatively small number of scattering centers, thus reducing the dimension of

the feature vector, and that these scattering centers have a direct physical interpretation.

The work by Chamberlain [8,9] presents a new way to examine full polarization data which provides a more complete description of a target's interaction with an incident radar wave. This work introduced the idea of a Transient Polarization Response (TPR), the backscattered response of a target illuminated with an impulse of circularly polarized radiation. The idea is that as the circularly polarized electromagnetic pulse strikes each scatterer on the target, the scatterer interacts with the pulse and sends a reflected wave back with a polarization which is determined by the configuration of that scatterer. The leading edge of a wing, for example, could be expected to return a horizontally polarized wave if it were illuminated from a nose-on aspect angle with no roll. This type of analysis provides a more complete and descriptive representation of the target than can be obtained from a single polarization signature. Not only are scattering centers and their energies determined, but also their polarization effects on a circularly polarized incident wave, which are in general elliptical. In reality a target is not a finite sum of discrete scattering centers but rather has a continuous TPR; thus, the TPR is examined where it has high energy content, and a scattering center (along with its polarization ellipse) is assigned to that point in the down range.

Chamberlain has developed FFT-based techniques for extracting scattering centers and their elliptical polarization returns [8]. This report extends his work to parametric modeling, which provides a higher resolution and a reduced set of data with which to identify a target. This offers some

advantages over the non-parametric technique in [8]. First, scattering center ranges and polarization ellipses are directly estimated. This eliminates the need for a knowledge-based scattering center extraction step used in the FFT-processing methods. Second, the parametric technique is capable of higher resolution than the FFT-based method, and can resolve closely spaced scattering mechanisms which the FFT-based methods cannot resolve. This latter point is especially important for low frequency radar applications and in high fidelity applications such as scattering analysis of objects where one wishes, for example, to separate a direct scattering component from a creeping wave component.

An outline of this report is as follows. In Chapter 2 the full polarization, exponential data model is introduced along with a procedure with which to find ranges and polarization ellipses from the model parameters. Chapter 3 presents an algorithm with which to find the parameters of the model. Chapter 4 presents simulation results from a simulated model, a simplified aircraft model, and scale models of real aircraft. Finally, Chapter 5 concludes the report.

Chapter 2

The Exponential Parametric Model of Target Signatures

Radar systems are typically designed to transmit horizontally and vertically polarized radiation and receive the horizontally and vertically polarized radar scattering coefficients at stepped frequencies in a certain bandwidth: $s_{hh}(f)$, $s_{vh}(f) = s_{hv}(f)$, and $s_{vv}(f)$ (see [3] for an explanation).

It is well known that the inverse Fourier Transform of these data gives a time or down range impulse response of the target [2]. The Fast Fourier Transform is often used to compute the impulse response from the scattering data. The frequency spacing and total bandwidth of the data control the resolution and range extent of the impulse response. Each of the various returns can be transformed from the frequency domain to the time (range) domain to provide down range information about a target. Various scattering mechanisms will affect the various returns appropriately in the frequency domain measurements and appear as impulsive responses in the range domain. These down range profiles can be arrived at via various FFT and parametric techniques. If these returns are coherent, then scattering

mechanisms will appear in one or more polarization returns and cause impulsive responses at the same range in the range domain. In this way the sets of data can be used together to identify scattering centers.

The full polarization model to be introduced uses the sets of data together not only to determine the ranges of scatterers, but also to determine the polarization of a return by each scatterer upon incidence of a circularly polarized wave. Thus, this type of analysis requires data which is circularly transmitted and horizontally and vertically received, $s_{hl}(f)$ and $s_{vl}(f)$. Left circular has been arbitrarily chosen since, on a macroscopic level, a target's features appear the same to both left and right circularly polarized transmit fields. Since what available data is horizontal and vertical transmit and receive, $s_{hl}(f)$ and $s_{vl}(f)$ are found using the following transformation [8]:

$$\begin{bmatrix} s_{hl}(f_k) \\ s_{vl}(f_k) \end{bmatrix} = \begin{bmatrix} s_{hh}(f_k) & s_{hv}(f_k) \\ s_{vh}(f_k) & s_{vv}(f_k) \end{bmatrix} \begin{bmatrix} 1 \\ j \end{bmatrix} \frac{1}{\sqrt{2}}. \tag{2.1}$$

The horizontal and vertical radar return from a target illuminated with stepped frequency circularly polarized radiation can each be modeled a sum of complex exponentials [6,7]. The scattering points of the target are thus the poles of these exponential models, and amplitudes associated with each pole represent the scatterer's horizontal and vertical return.

As mentioned before, one approach to multi-polarized signal analysis is to use exponential modeling on the horizontally and the vertically polarized received data independently. This model can then be used to identify the target [2,6,7]. However, it is reasonable to assume that for circularly polarized transmitted waves, if a scattering center appears in the horizontal return, then it is also present in the vertical return. Thus, when estimating

the scatterers of the model, both the horizontal and vertical information can be used simultaneously to estimate the ranges of the scattering centers. The target's horizontal and vertical impulse response to left circularly polarized radiation can be modeled as a function of range (time) r as follows [7]:

$$\begin{bmatrix} s_{hl}(r) \\ s_{vl}(r) \end{bmatrix} = \sum_{k=1}^{M} \begin{bmatrix} a_{hk} \\ a_{vk} \end{bmatrix} \frac{1}{e^{-j2\pi r/R} - p_k} \qquad 0 \le r \le R \tag{2.2}$$

where R is the maximum unambiguous range which is given by

$$R = \frac{c}{2\Delta f}. \tag{2.3}$$

The inverse Fourier transform of equation (2.2) leads to the following frequency domain model for the radar return signals at N frequency measurements:

$$\begin{bmatrix} s_{hl}(f) \\ s_{vl}(f) \end{bmatrix} = \sum_{k=1}^{M} \begin{bmatrix} a_{hk} \\ a_{vk} \end{bmatrix} p_k^f \qquad f = 1, \ldots, N. \tag{2.4}$$

Here, it is assumed that there are M scattering centers. Each p_k is a scattering center pole; its angle corresponds to the range of the scattering center, and its magnitude corresponds to a frequency dependent return from the scatterer. Each a_{hk} is the horizontal amplitude associated with that pole, and a_{vk} is the vertical amplitude associated with the same pole. For an ideal point scatterer, $|p_k| = 1$, but for more realistic targets it is useful to assume that the scattering will be attenuated slightly as frequency either increases or decreases, thus $|p_k|$ will vary a little bit around one. These scattering centers cause peaks in the TPR (a time domain response) which correspond to the ranges (times) at which the incident wave is reflected. From equation (2.2) it can be seen that this occurs at the angles at which these poles are located and thus the ranges of these scattering centers are

related to the angles at which the poles are located; if $\angle p_k$ is the angle of the kth pole, then the (relative) range of the scattering center is given by

$$r_k = R\frac{\angle p_k}{2\pi}. \tag{2.5}$$

The fact that the angle of a pole can only be between 0 and 2π radians corresponds to an unambiguous range R.

2.1 Determining Scattering Center Locations and Polarizations

Once the model has been determined, the angle at which the poles appear represent the down range location of each of the scatterers according to equation (2.5). The horizontal and vertical amplitudes associated with each pole contain the information about polarization characteristics of each scattering center. These response polarizations are in general elliptical and, along with the ranges of the scattering centers, can be used to identify the target.

Now, from a_{hi}, a_{vi}, and p_i, for each scatterer i, its range r_i and its polarization in terms of tilt τ_i, ellipticity ϵ_i, and major axis A_i can be determined. They are given by equation (2.5) and the following equations [8,10]:

$$\tau_i = \frac{1}{2}\tan^{-1}\left(\tan\left(2\gamma_i\right)\cos\left(\delta_i\right)\right) \tag{2.6}$$

$$\epsilon_i = \frac{1}{2}\sin^{-1}\left(\frac{\sin\left(2\gamma_i\right)}{\sin\left(\delta_i\right)}\right) \tag{2.7}$$

where

$$\gamma_i = \tan^{-1}\left(\frac{E_{2i}}{E_{1i}}\right) \tag{2.8}$$

$$\delta_i = \angle a_{vi} - \angle a_{hi} \tag{2.9}$$

$$E_{1i} = |a_{hi}|\,, \qquad E_{2i} = |a_{vi}|\,. \tag{2.10}$$

The above calculations lead to use of only one fourth of the Poincare polarization sphere. To avoid this ambiguity, the following alterations to the tilt need to be made [8]:

$$\tau_i = \tau_i + \frac{\pi}{2} \quad \text{if } \gamma_i > \frac{\pi}{4} \tag{2.11}$$

$$\tau_i = \tau_i + \frac{\pi}{2} \quad \text{if } \gamma_i \leq \frac{\pi}{4} \text{ and } \tau_i < 0. \tag{2.12}$$

To determine the length of the major axis, A_i, the ellipse can be rotated by its tilt τ_i so that the ellipse axes align with the horizontal and vertical axes as follows [8]:

$$\begin{bmatrix} E'_{1i} \\ E'_{2i} \end{bmatrix} = \begin{bmatrix} \cos(\tau_i) & \sin(\tau_i) \\ -\sin(\tau_i) & \cos(\tau_i) \end{bmatrix} \begin{bmatrix} E_{1i} \\ E_{2i}e^{j\delta_i} \end{bmatrix}. \tag{2.13}$$

And thus the major axis is given by

$$A_i = |E'_{1i}|\,. \tag{2.14}$$

This set of parameters $\{r_i, \tau_i, \epsilon_i, A_i; i = 1, \ldots, M\}$ now provides a concise description of the target. This parameter set characterizes a target as a set of M scattering centers, each one described by its range and a polarization ellipse of the scattered energy. The ranges of a target's scatterers and their respective polarization characteristics can then be used as features in a target recognition system.

Chapter 3

Estimating The Exponential Parametric Model From Data

This chapter presents an algorithm for estimating the model parameters in equations (2.4)–(2.14) from scattering center data. A modification of the algorithm to expand the target to fill a significant portion of the unambiguous range R is also presented.

The algorithm consists of three steps. First, the poles are estimated using linear prediction. Next, the amplitude terms are estimated using a least squares technique. Finally, the amplitude terms are converted into polarization ellipse parameters which describe the TPR of each scattering center.

The first two steps involve estimating the poles and amplitudes of a damped exponential model. This problem has been well-studied in the time series analysis literature [11,12], and successful algorithms for single polarization data have been developed [7]. The algorithm below represents a generalization of the one in [7] for the full polarization data case.

First, the poles are estimated using backward linear prediction coupled with least squares [11,12,13]. The backward linear prediction equations can be written as follows:

$$\begin{bmatrix} s_{hl}(1) & s_{hl}(2) & s_{hl}(3) & \cdots & s_{hl}(L+1) \\ s_{hl}(2) & s_{hl}(3) & & & \vdots \\ \vdots & \vdots & & & \vdots \\ s_{hl}(N-L) & s_{hl}(N-L+1) & \cdots & \cdots & s_{hl}(N) \\ s_{vl}(1) & s_{vl}(2) & s_{vl}(3) & \cdots & s_{vl}(L+1) \\ s_{vl}(2) & s_{vl}(3) & & & \vdots \\ \vdots & \vdots & & & \vdots \\ s_{vl}(N-L) & s_{vl}(N-L+1) & \cdots & \cdots & s_{vl}(N) \end{bmatrix} \begin{bmatrix} 1 \\ \hat{b}_1 \\ \vdots \\ \hat{b}_L \end{bmatrix} = 0 \quad (3.1)$$

or

$$S\hat{b} = -s \tag{3.2}$$

where L is the order of prediction, and $\hat{b}$ is the coefficient vector of the polynomial $\hat{B}(z)$ given by

$$\hat{B}(z) = 1 + \hat{b}_1 z^{-1} + \cdots + \hat{b}_L z^{-L}. \tag{3.3}$$

Note that both the $s_{hl}(f)$ and $s_{vl}(f)$ sets of data are used simultaneously to estimate a single set of prediction coefficients.

Ideally, L can be any integer greater than or equal to the model order M; in practice, choosing $L > M$ results in more accurate parameter estimates.

The solution of equation (3.1) involves forming the matrix $[s : S]$, performing a singular value decomposition (SVD) on it, then truncating all but the first M singular values, to arrive at a noise cleaned estimate $\left[\hat{s} : \hat{S}\right]$ [13]. Next, the linear prediction coefficient vector $\hat{\hat{b}}$ is found as:

$$\hat{\hat{b}} = -\hat{S}^{+}\hat{s} \tag{3.4}$$

where the $^+$ denotes pseudoinverse. Finally, the estimated poles can be determined as:

$$\hat{p}_i = \frac{1}{\text{root}_i\left(\hat{\hat{B}}(z)\right)} \qquad i = 1, \ldots, L. \tag{3.5}$$

Since distinguishing scatterers result in peaky responses, those poles which do not lie within a given annular region about the unit circle can be eliminated from the model. The following criterion has been found to work well for radar data [7]:

$$\frac{1}{100} < |\hat{p}_i|^N < 100. \tag{3.6}$$

This criterion discards any scattering centers whose response energy differs by more than 40 dB from the lowest to highest measured frequency. Only those poles in equation (3.5) which satisfy equation (3.6) are kept.

Once these L' poles have been determined, the amplitude equations for both the horizontal and vertical components can be formed. From equation (2.4),

$$\begin{bmatrix} \hat{p}_1^1 & \cdots & \hat{p}_{L'}^1 \\ \vdots & & \vdots \\ \hat{p}_1^N & \cdots & \hat{p}_{L'}^N \end{bmatrix} \begin{bmatrix} \hat{a}_{h1} & \hat{a}_{v1} \\ \vdots & \vdots \\ \hat{a}_{hL'} & \hat{a}_{vL'} \end{bmatrix} = \begin{bmatrix} s_{hl}(1) & s_{vl}(1) \\ \vdots & \vdots \\ s_{hl}(N) & s_{vl}(N) \end{bmatrix} \tag{3.7}$$

or

$$\hat{P}\hat{A} = S_a. \tag{3.8}$$

The amplitudes can be found from a least squares solution to equation (3.8)

$$\hat{A} = \left(\hat{P}^H \hat{P}\right)^{-1} \hat{P}^H S_a. \tag{3.9}$$

Since only M singular values were kept, no more than M of these scatterers can be anything but noise. Therefore the L'' scatterers with the

largest axis diagonal (energy) should be kept, where

$$L'' = \min\{M, L'\}. \tag{3.10}$$

3.1 Expanding the Target to Fill the Unambiguous Range

In certain cases the spacing Δf of the given frequency data is so small that the unambiguous range given by equation (2.3) is large compared to the size of the target. If this occurs, then details of the target can be lost because the resolution is lower. To avoid this, the data can be decimated by a factor d when a frequency spacing of $d\Delta f$ would be more appropriate in order to make the target fill a significant portion of the unambiguous range.

In the formation of $[s : S]$ (see equation (3.2)) the data should be decimated. Thus, equation (3.1) is replaced by

$$\begin{bmatrix} s_{hl}(1) & s_{hl}(1+d) & \cdots & s_{hl}(1+Ld) \\ s_{hl}(2) & s_{hl}(2+d) & & s_{hl}(2+Ld) \\ \vdots & \vdots & & \vdots \\ s_{hl}(N-Ld) & s_{hl}(N-Ld+d) & \cdots & s_{hl}(N) \\ s_{vl}(1) & s_{vl}(1+d) & \cdots & s_{vl}(1+Ld) \\ s_{vl}(2) & s_{vl}(2+d) & & s_{vl}(2+Ld) \\ \vdots & \vdots & & \vdots \\ s_{vl}(N-Ld) & s_{vl}(N-Ld+d) & \cdots & s_{vl}(N) \end{bmatrix} \begin{bmatrix} 1 \\ \hat{b}_1 \\ \vdots \\ \hat{b}_L \end{bmatrix} = 0. \tag{3.11}$$

Since the estimated poles from equation (3.11) have a decay rate d times faster than the actual data requires, equation (3.6) becomes

$$\frac{1}{100} < |\hat{p}_i|^{\frac{N}{d}} < 100. \tag{3.12}$$

and equation (3.7) becomes

$$\begin{bmatrix} \hat{p}_1^{\frac{1}{d}} & \cdots & \hat{p}_{L'}^{\frac{1}{d}} \\ \vdots & & \vdots \\ \hat{p}_1^{\frac{N}{d}} & \cdots & \hat{p}_{L'}^{\frac{N}{d}} \end{bmatrix} \begin{bmatrix} \hat{a}_{h1} & \hat{a}_{v1} \\ \vdots & \vdots \\ \hat{a}_{hL'} & \hat{a}_{vL'} \end{bmatrix} = \begin{bmatrix} s_{hl}(1) & s_{vl}(1) \\ \vdots & \vdots \\ s_{hl}(N) & s_{vl}(N) \end{bmatrix}. \tag{3.13}$$

Any noisy response which occurred before or after the target in the range domain could now be subject to foldover when this decimation is performed. To avoid this problem the data should be filtered to eliminate any extraneous noisy responses before they are folded over into the target's response.

Chapter 4

Simulation Results

This chapter presents results obtained by applying the exponential modeling algorithm to various sets of data. First, a simulated point scattering model of data is used. Then, results of the algorithm as applied to compact range measurements of a simplified aircraft model and scale models of real aircraft are presented.

4.1 Simulated Point Scatterer Model

In this experiment, scattering data which corresponds to an ideal point scatterer model of an aircraft as shown in Figure 4.1 was generated. This model, proposed in [8], consists of four scattering centers at the nose, wing tips, horizontal stabilizers, and tail. The ranges of the scattering centers are at 0.00, 8.96, 14.9, and 15.2 cm down range with respect to the (reference) nose as shown in Figure 4.1. The scattering response for the nose is circular and is linear for the other three centers. The aircraft was rolled 10°, so, for example, the wing scattering response is linearly polarized at a 10° angle. The full polarization scattering matrix ($s_{hh}(f)$, $s_{hv}(f) = s_{vh}(f)$, and $s_{vv}(f)$)

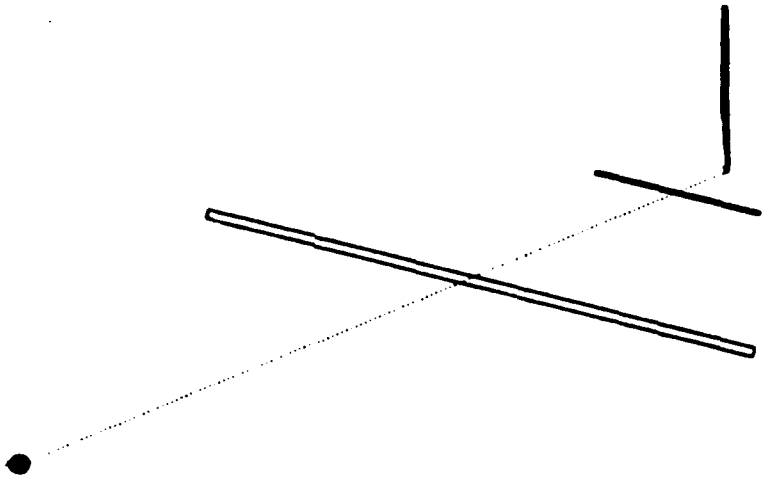

Figure 4.1: Ideal Model

for each frequency between 2 and 18 GHz in 50 MHz steps was generated by summing up the responses for each scatterer as given in Table 4.1.

The horizontal and vertical scattering data was first converted to a left circularly polarized transmit basis using equation (2.1). Then, the resulting scattering data was applied to the exponential modeling algorithm using $L = 10$ with the following modification. In order to keep the unambiguous range R near the target size, the frequency spacing between measurements should be about 500 MHz, not 50 MHz. To obtain this frequency spacing, the scattering data is decimated by a factor of $d = 10$ according to equation (3.11). The results of the modeling for $M = 4$ and for $M = 3$ are summarized by Table 4.2 and are discussed below.

The results of the modeling for $M = 4$ are shown in Figure 4.2. The range scale is in meters. It can be seen that the four scattering centers are accurately estimated. Moreover, the amplitude and polarization of each scattering center are also estimated very accurately. Note that the

Table 4.1: Ideal Model Data Equations

Scatterer	$\begin{bmatrix} s_{hh}(f) & s_{hv}(f) \\ s_{vh}(f) & s_{vv}(f) \end{bmatrix}$
Nose	$\begin{bmatrix} 1 & 0 \\ 0 & 1 \end{bmatrix} e^{-j4\pi 7.38 f/c}$
Wing	$\begin{bmatrix} \cos^2(10°) & \frac{\sin(20°)}{2} \\ \frac{\sin(20°)}{2} & \sin^2(10°) \end{bmatrix} 10e^{-j4\pi 16.3 f/c}$
Stabilizer	$\begin{bmatrix} \cos^2(10°) & \frac{\sin(20°)}{2} \\ \frac{\sin(20°)}{2} & \sin^2(10°) \end{bmatrix} 2e^{-j4\pi 22.3 f/c}$
Tail	$\begin{bmatrix} \sin^2(10°) & -\frac{\sin(20°)}{2} \\ -\frac{\sin(20°)}{2} & \cos^2(10°) \end{bmatrix} 3e^{-j4\pi 22.6 f/c}$

Table 4.2: Ideal Model Parameters

	True Value				M=4 Estimate				M=3 Estimate			
Scat.	$\tau(°)$	$\epsilon(°)$	A	r(cm)	$\hat{\tau}(°)$	$\hat{\epsilon}(°)$	$\hat{A}$	$\hat{r}$(cm)	$\hat{\tau}(°)$	$\hat{\epsilon}(°)$	$\hat{A}$	$\hat{r}$(cm)
Nose	-	45.0	.707	7.38	119	45.0	.707	7.38	100	44.1	.718	7.38
Wing	10.0	0.00	7.07	16.3	10.0	0.00	7.07	16.3	10.1	−0.04	7.10	16.3
Stab.	10.0	0.00	1.41	22.3	10.0	0.00	1.41	22.3	131	8.13	2.40	22.5
Tail	100	0.00	2.12	22.6	100	0.00	2.12	22.6				

horizontal stabilizer and tail are too close in range to be resolved by Fourier-based methods [8]; however, with the exponential modeling method these two scattering centers can be resolved.

If $M = 3$ in the algorithm, then at most three scattering centers can be identified, as is shown in Figure 4.3. The nose and wing scattering centers are accurately estimated as before, and the tail-horizontal stabilizer region is modeled as a single scattering center. Note that the polarization ellipse of the tail region is estimated at 15.1 cm from the nose, which is what one might expect for a combination of the two orthogonal linearly polarized responses. This plot shows that even when the number of scattering centers in the data exceeds the number that can be modeled, the algorithm generates an estimate which combines closely spaced scattering centers into one conglomerate scattering center. This is an important and desirable characteristic of the algorithm, as radar targets often contain a large number of scattering centers, not all of which can be individually estimated.

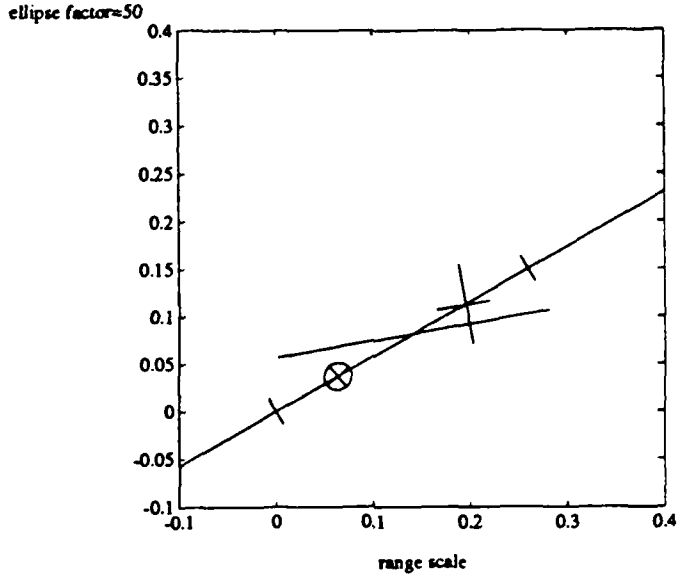

Figure 4.2: Ideal Model Scatterers and Polarizations, M=4

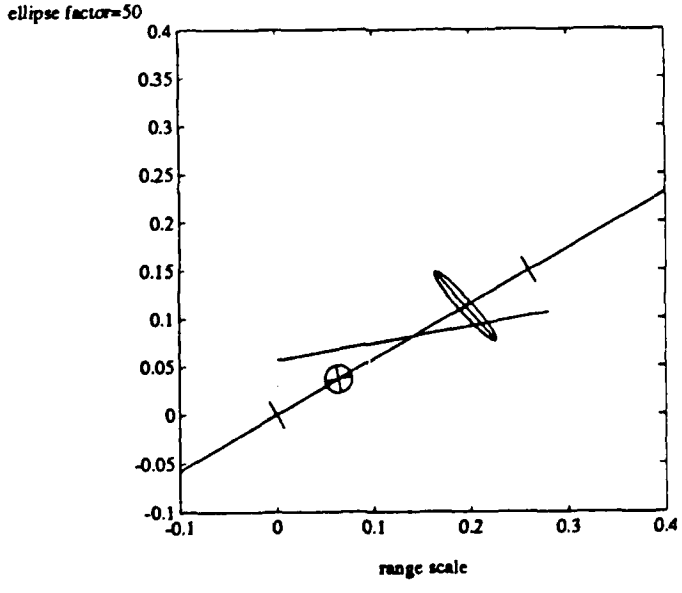

Figure 4.3: Ideal Model Scatterers and Polarizations, M=3

4.2 Simplified Aircraft Measurements

Next the exponential modeling procedure was applied to compact range measurements of a simplified, configurable aircraft target 6 inches (15.24 cm) in length. This target consists of a cylindrical fuselage (F) with removable wings (W), horizontal stabilizers (S), and tail (T); its plan view appears in Figure 4.4.

Compact range measurements of this model were taken with various parts removed. These configurations are shown in Figure 4.5. Each measurement set consists of full polarization measurements at frequencies between 2 and 18 GHz in 50 MHz steps from a nose-on aspect angle with no roll. The data was decimated by a factor of $d = 10$ as in equation (3.11) when applied to the exponential modeling algorithm. The model order was chosen as 10 and the number of singular which were kept varied from 3 to 7 depending on the complexity of the target. The values of L and M were arrived at in each case by experimentation. Several simulations were run for various values of L and M and, by observation, a medium was found between missing significant scatterers and allowing smaller spurious ones to appear. By comparing each target silhouette and its plan view with its corresponding estimated response, one can note that the estimated scattering centers correspond well to target geometry.

Figures 4.6–4.13 show the estimated scattering responses for the various configurations of the aircraft. Again, the range scale is in meters. By comparing each target silhouette in Figure 4.4 with its corresponding estimated response, one can note that the estimated scattering centers correspond well

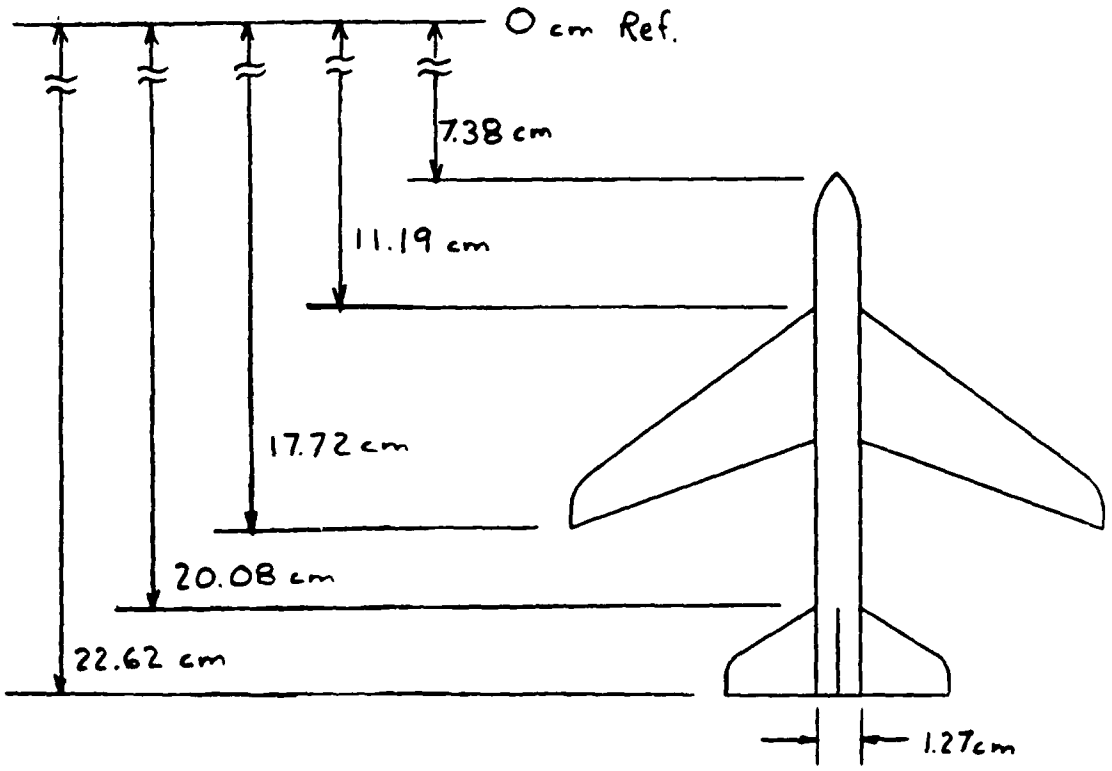

Figure 4.4: FWST Plan View

to target geometry. From all these figures it can be seen that the nose scattering is accurately estimated as a circularly polarized response. The two scattering responses at the end of the fuselage-only configuration in Figure 4.6 correspond to the scattering from the end of the cylinder and the creeping wave response which travels along the cylinder, along the disk at the back end, and back toward the front (delayed by one-half the cylinder diameter to account for the two-way propagation delay).

The two scatterers at the end of the fuselage-tail configuration in Figure 4.7 correspond to the leading and trailing edge of the tail. Note the strong vertical polarization of the leading edge and the more circularly po-

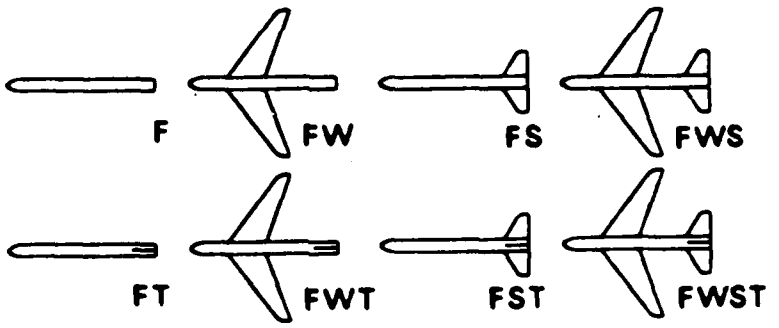

Figure 4.5: Simple Targets

larized trailing edge response. The latter is probably due to a combination of the tail trailing edge and the cylindrical trailing edge. Similar conclusions can be seen in the fuselage-stabilizer estimate in Figure 4.8. Here the leading edge of the stabilizers is seen as a strongly linear, horizontal polarization response. The two tail responses correspond to the trailing edge of the fuselage-cylinder and to the creeping wave response (delayed by one-half the cylinder diameter to account for the two-way propagation delay).

The fuselage-stabilizer-tail configuration in Figure 4.9 has a scatterer corresponding to the leading and trailing edges of the stabilizer and tail, along with a response due to a creeping wave along their edges. Note that the height and width of the rear polarizations are at a ratio of $1 : 2$ which agrees with the fact that the stabilizer is twice as long as the tail. The reason why the ellipses are much larger in this response

than in the others is not known at this time. In a dB sense they are not that much larger than the others anyway.

The fuselage-wing configuration result in Figure 4.10 clearly shows the circular nose response, a small horizontal scattering term at the leading corners of the wing, and a horizontal term at the trailing tips of the wing. Next there is a small horizontally polarized scattering term which may be caused by a creeping wave response. The final scattering center corresponds to the trailing edge of the fuselage. This response is more vertically polarized than the response in Figure 4.6 (from the geometry one would expect it to be circularly polarized). The vertical polarization may result because most of the horizontally polarized signal was reflected by the wing, leaving mostly vertically polarized energy to be incident on the cylinder trailing edge. Neither the addition of the tail in Figure 4.11 nor the stabilizer in Figure 4.12 nor both in Figure 4.13 affect the locations of scattering centers, but they do alter the polarizations of the rear scatterers.

The more complicated configurations in general correspond less to the target geometry towards the rear of the target. However, the primary scattering centers for the more complicated target configurations are still well-estimated. The polarization of these scattering centers correspond less well to the target geometry than for simpler configurations, especially near the tail of the target. In all cases, though, the primary scattering centers are accurately located.

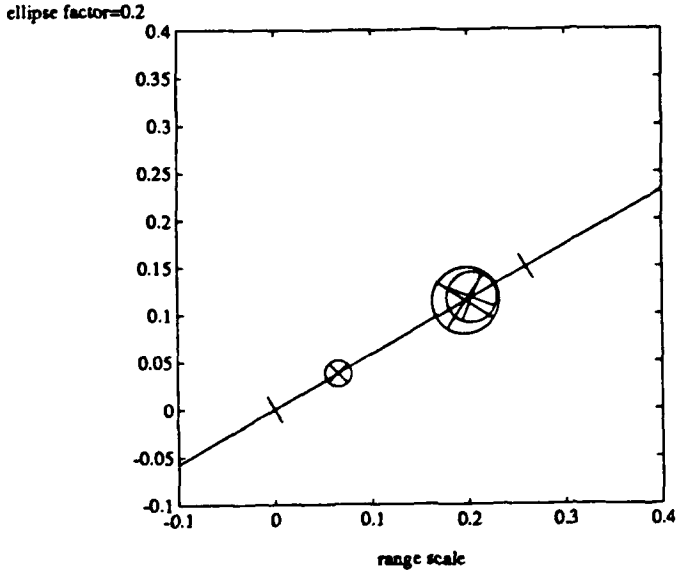

Scatterer	$\hat{r}$(cm)
1	7.58
2	22.8
3	23.6

Figure 4.6: F Scatterers and Polarizations

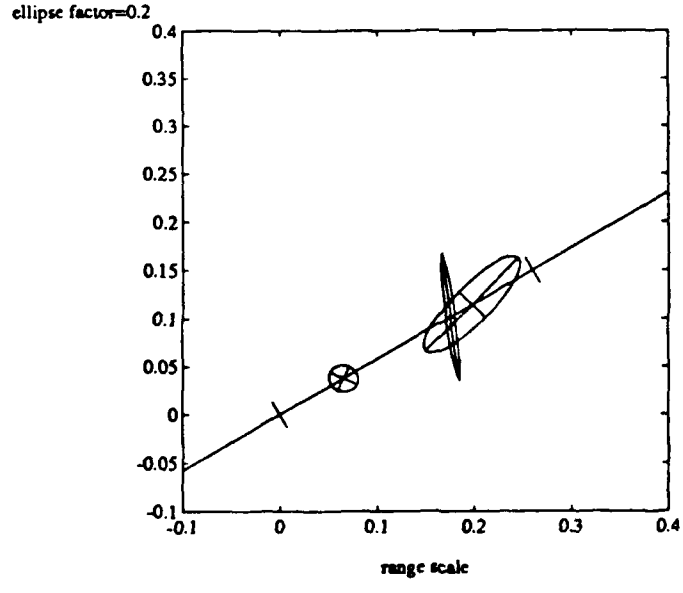

Scatterer	$\hat{r}$(cm)
1	7.53
2	20.3
3	22.8

Figure 4.7: FT Scatterers and Polarizations

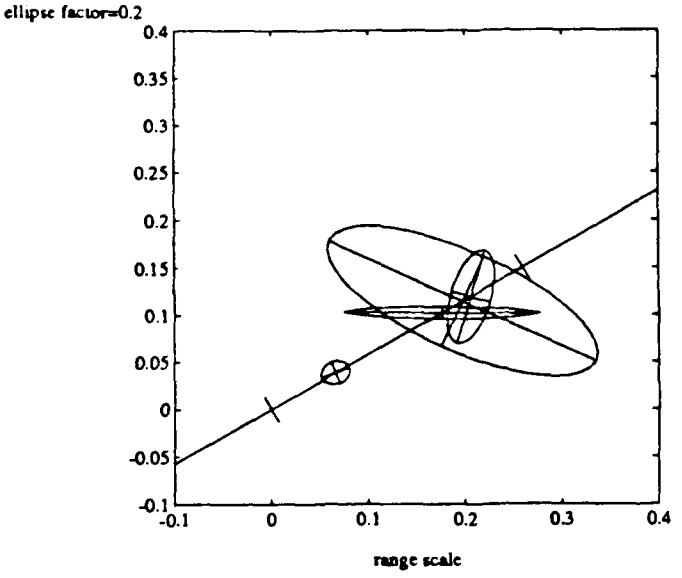

Scatterer	$\hat{r}$(cm)
1	7.68
2	20.4
3	22.8
4	23.8

Figure 4.8: FS Scatterers and Polarizations

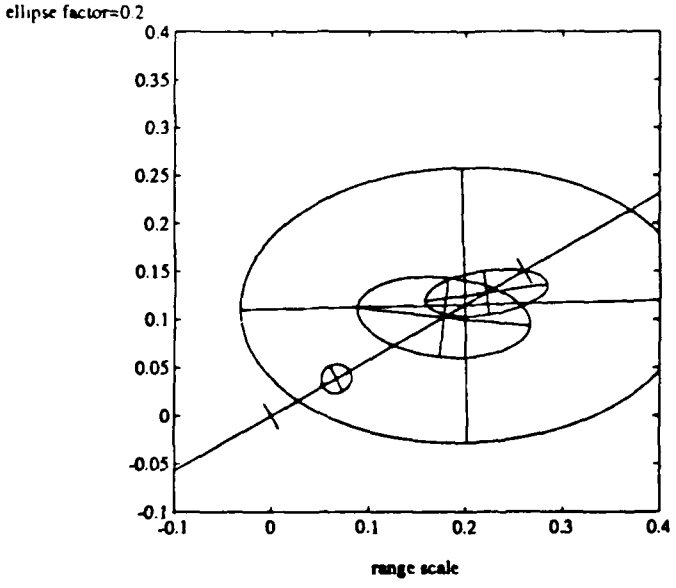

Scatterer	$\hat{r}$(cm)
1	7.72
2	20.5
3	23.0
4	25.5

Figure 4.9: FST Scatterers and Polarizations

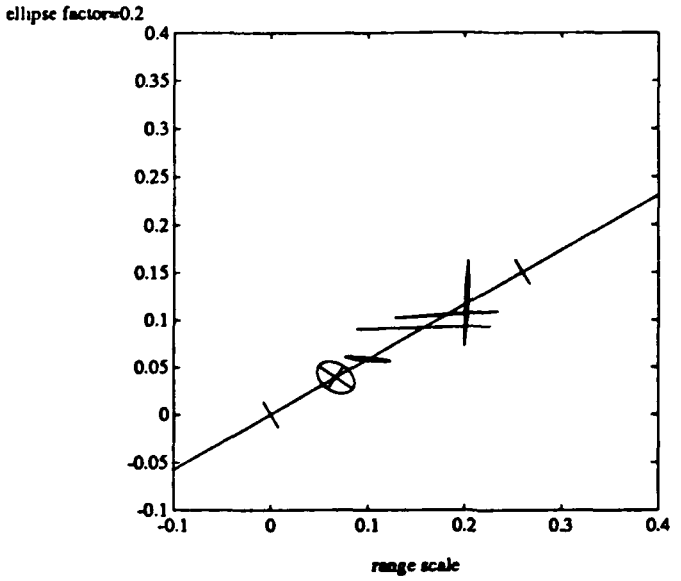

Scatterer	$\hat{r}$(cm)
1	7.76
2	11.7
3	18.3
4	21.0
5	23.3

Figure 4.10: FW Scatterers and Polarizations

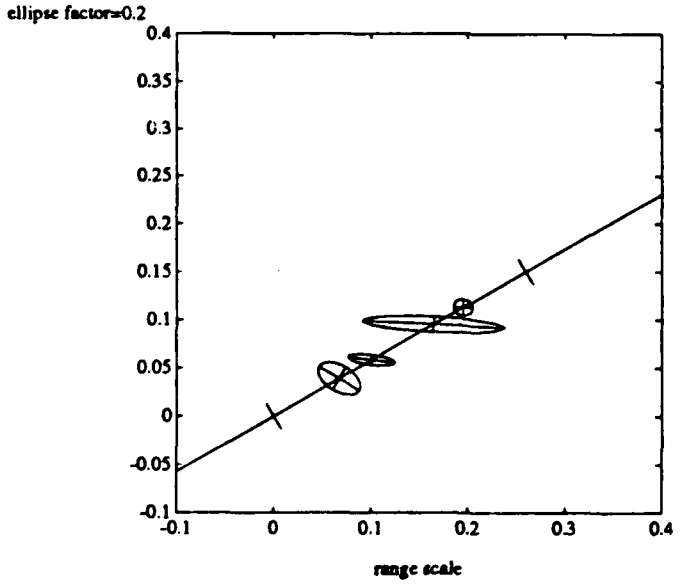

Scatterer	$\hat{r}$(cm)
1	7.80
2	11.7
3	19.1
4	22.5

Figure 4.11: FWT Scatterers and Polarizations

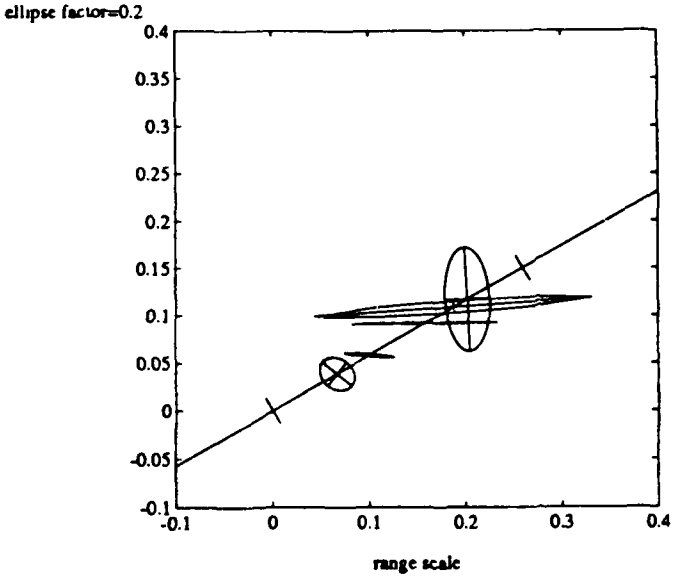

Scatterer	$\hat{r}$(cm)
1	7.73
2	11.6
3	18.3
4	21.7
5	23.3

Figure 4.12: FWS Scatterers and Polarizations

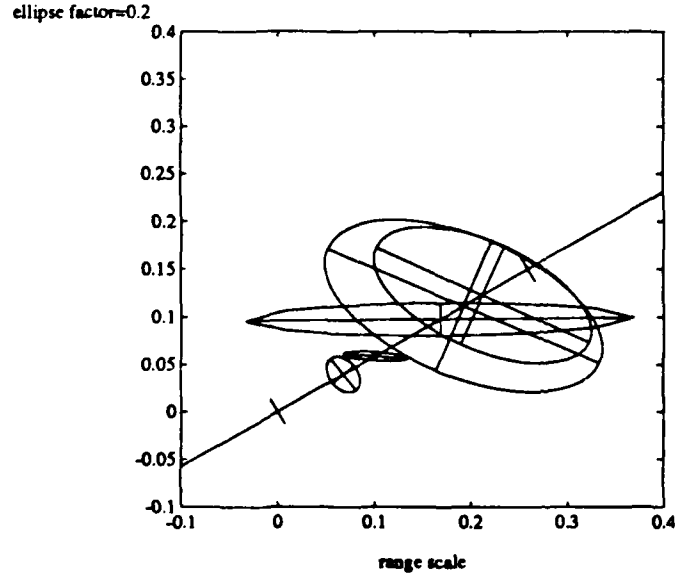

Scatterer	$\hat{r}$(cm)
1	7.92
2	11.7
3	19.5
4	22.3
5	24.6

Figure 4.13: FWST Scatterers and Polarizations

4.3 Scale Model Aircraft Measurements

In this section, the results of modeling scale models of five commercial aircraft (the Boeing 707, 727, 747, and DC10 and the Concord) are presented. These models measure from 23 to 43 cm in length. Eighty measurements $s_{hh}(f)$, $s_{vh}(f) = s_{hv}(f)$, and $s_{vv}(f)$ on the scale models are taken for frequencies between 6.45 and 10.4 GHz in 50 MHz steps from a nose-on aspect angle with no roll. The models are scaled between 130 and 200 so these results correspond to measurements in the HF band (30 to 90 MHz) for the full sized aircraft. To achieve an unambiguous range of 75 cm, the data was decimated by a factor of $d = 4$ as in equation (3.11) in the estimation procedure. A model order 10 was chosen with 5 singular values kept for all the following simulations of the model aircraft (they were chosen through experimentation as with the simplified aircraft). Figure 4.14 shows the plan views of each aircraft. Figure 4.15 shows the five aircraft silhouettes in the same scale as the estimation figures which follow. Figures 4.16–4.20 show the estimated responses for each aircraft with no noise. By comparing each target silhouette and its plan view with its corresponding estimated response, one can note that the estimated scattering centers correspond well to target geometry. Specifically, the nose, cockpit cavity, leading edge of wings, and engine inlets are all located for most of the models. Because of the calibration procedure used, the zero reference point is not known exactly; thus, the target could be positioned slightly differently than shown. Also, the electromagnetic mechanism of the scattering centers is not precisely known, and thus, the exact point in an engine inlet, for example, at

which the scattering occurs is also not known. These may account for some of the errors in the range estimates of scatterers and the ranges depicted in the plan views.

To examine the effects of noise on the estimate, Figures 4.21–4.35 show results of each aircraft model in 10, 5, and 0 dB SNR, respectively. In each case, independent white noise was added to each term of the scattering matrix (in left circular coordinates). Five different estimates obtained from five different noise realizations are shown overlapped in these figures. Two plots of each estimate is shown. The first is the polarization ellipse versus range plot as shown earlier. The second plot shows the magnitude of each ellipse (i.e., the hypotenuse between the major and minor axes) versus range. This plot can be viewed as a projection of the first plot. In the second plot, the tilt angle and ellipticity of the polarization is lost in the projection.

From these figures it can be seen that at 10 dB SNR the estimates show little deviation from the noiseless estimate (compare Figure 4.30 with Figure 4.19, for example). As the SNR is reduced to 0 dB, the major scattering centers are still estimated; however, the accuracy of the range, amplitude, ellipticity, and tilt decreases somewhat (as is expected). Some spurious estimates are seen but these have small magnitudes compared to the actual scattering center magnitudes. The results for each plane are comparable—the 707 and Concord estimates show a little less sensitivity to noise than do the 727 and DC10 estimates. The 747 polarization estimates are quite sensitive, but its range estimates are as robust as any of the other aircraft.

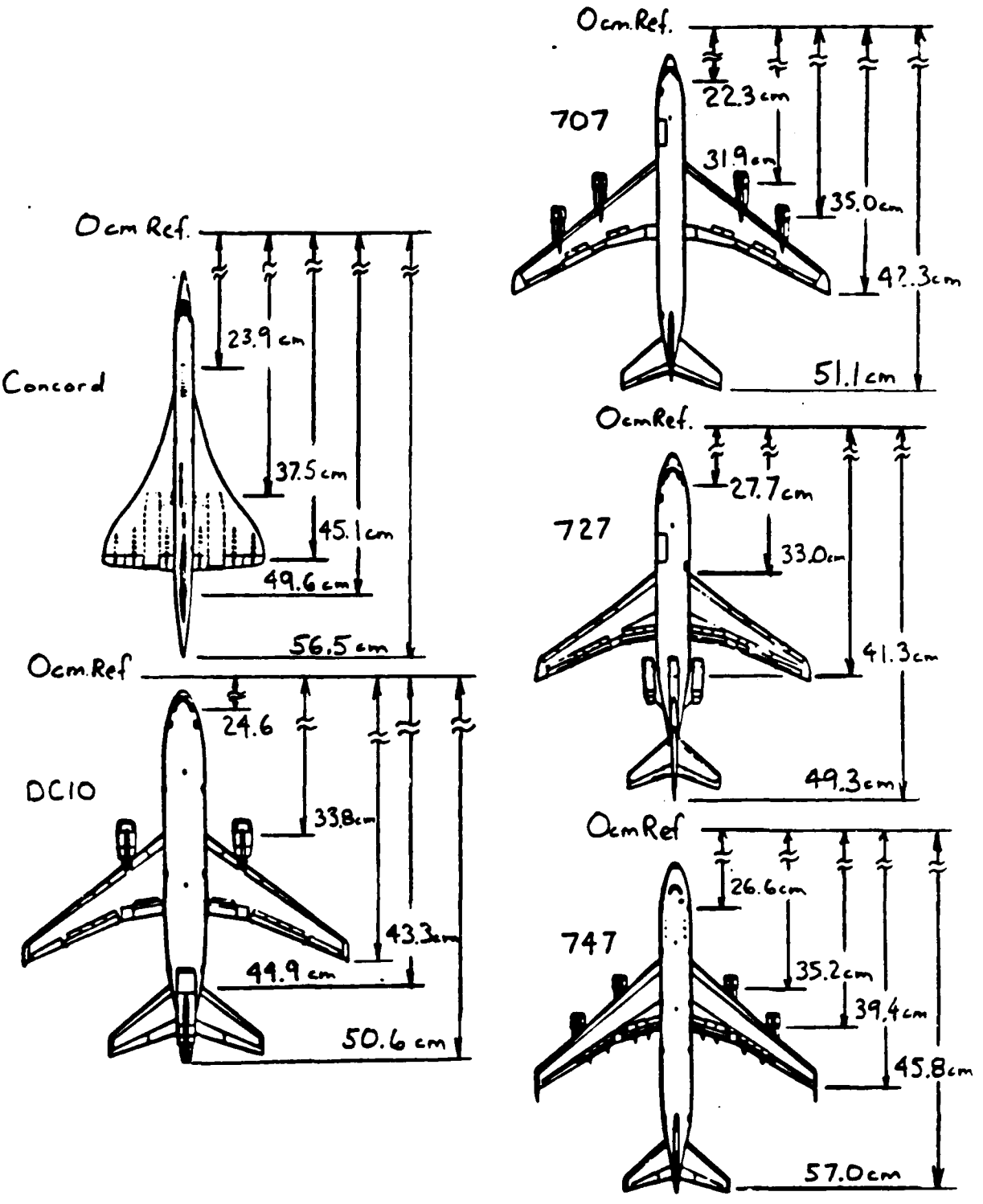

Figure 4.14: Model Aircraft Plan Views

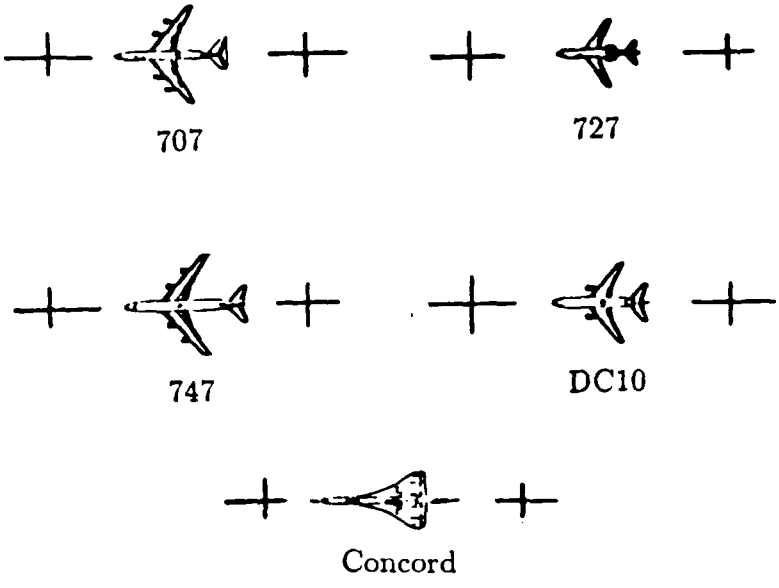

Figure 4.15: Model Aircraft

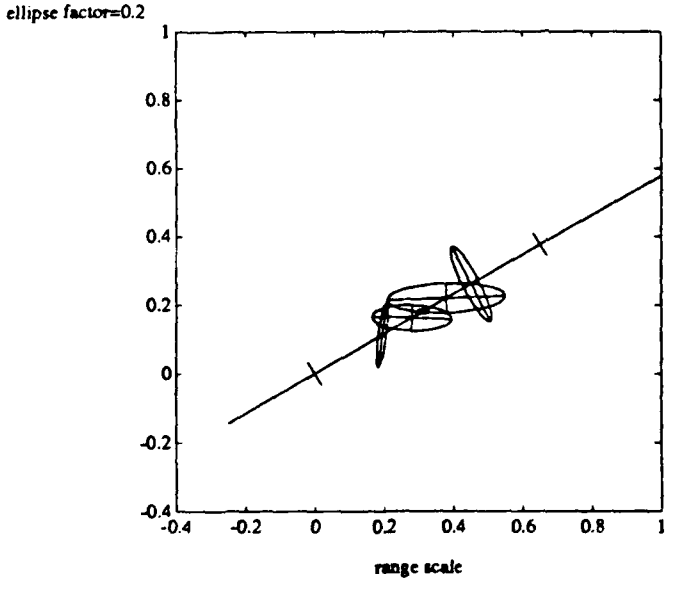

Scatterer	$\hat{r}$(cm)
1	22.5
2	32.3
3	36.0
4	43.8
5	52.0

Figure 4.16: 707 Scatterers and Polarizations

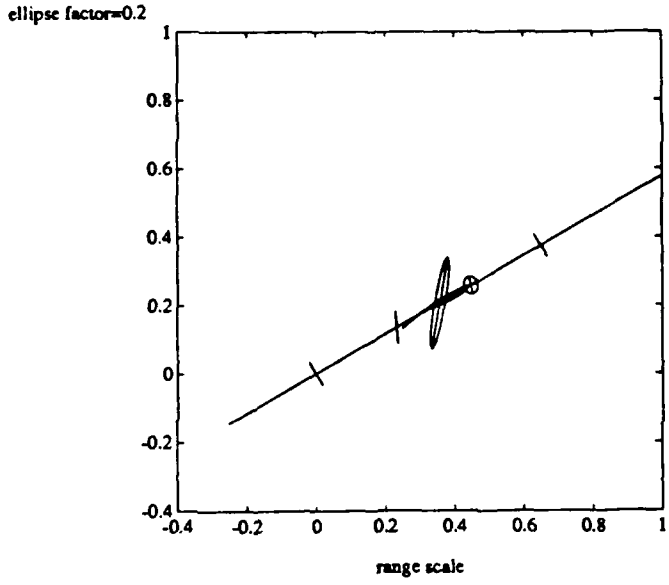

Scatterer	$\hat{r}$(cm)
1	27.0
2	34.8
3	41.3
4	45.0
5	51.6

Figure 4.17: 727 Scatterers and Polarizations

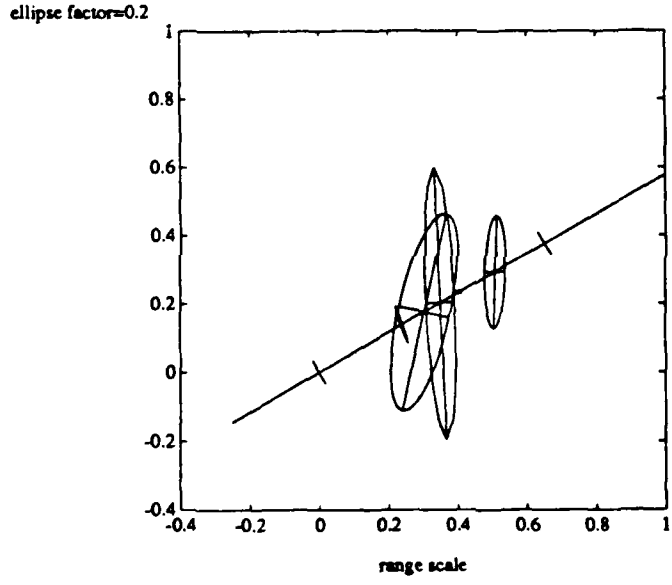

Scatterer	$\hat{r}$(cm)
1	27.6
2	35.0
3	40.4
4	46.6
5	58.7

Figure 4.18: 747 Scatterers and Polarizations

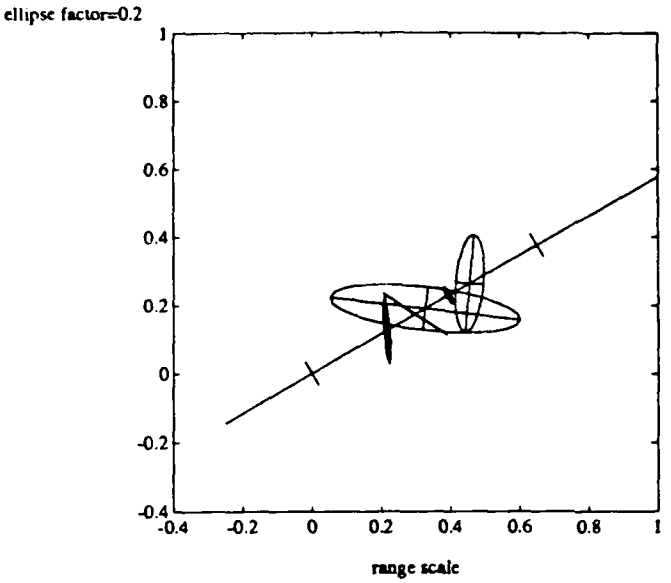

Scatterer	$\hat{r}$(cm)
1	25.0
2	34.5
3	37.8
4	45.5
5	52.6

Figure 4.19: DC10 Scatterers and Polarizations

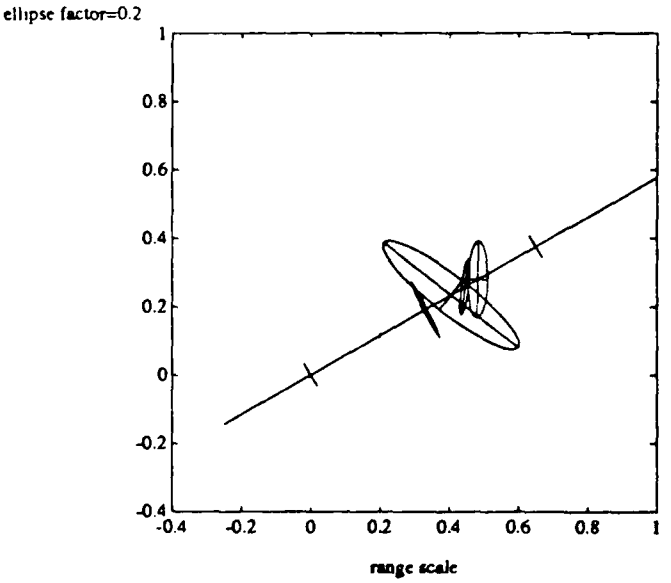

Scatterer	$\hat{r}$(cm)
1	23.1
2	38.2
3	46.8
4	51.5
5	55.7

Figure 4.20: Concord Scatterers and Polarizations

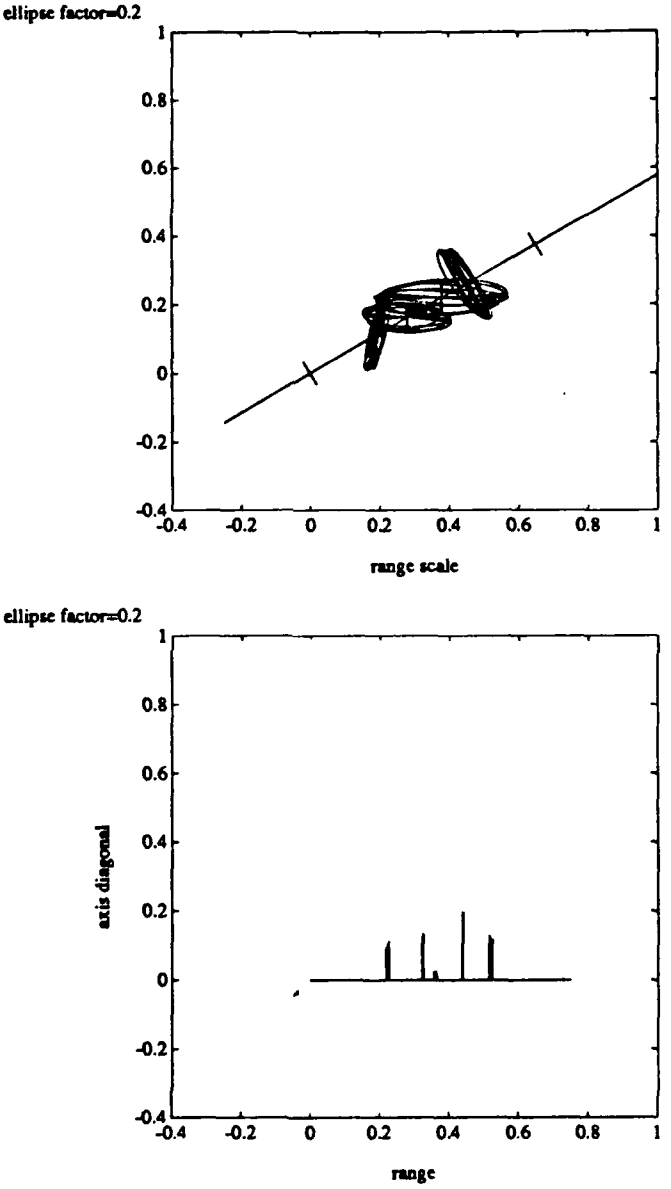

Figure 4.21: 707 Scatterers and Polarizations, SNR of 10dB

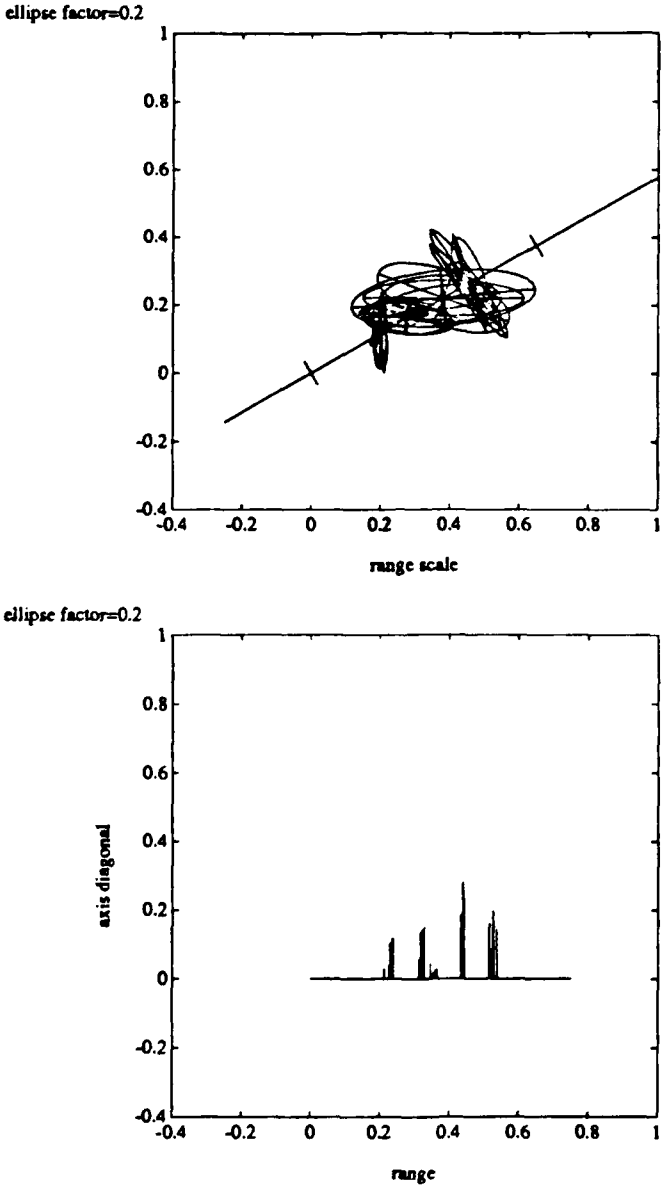

Figure 4.22: 707 Scatterers and Polarizations, SNR of 5dB

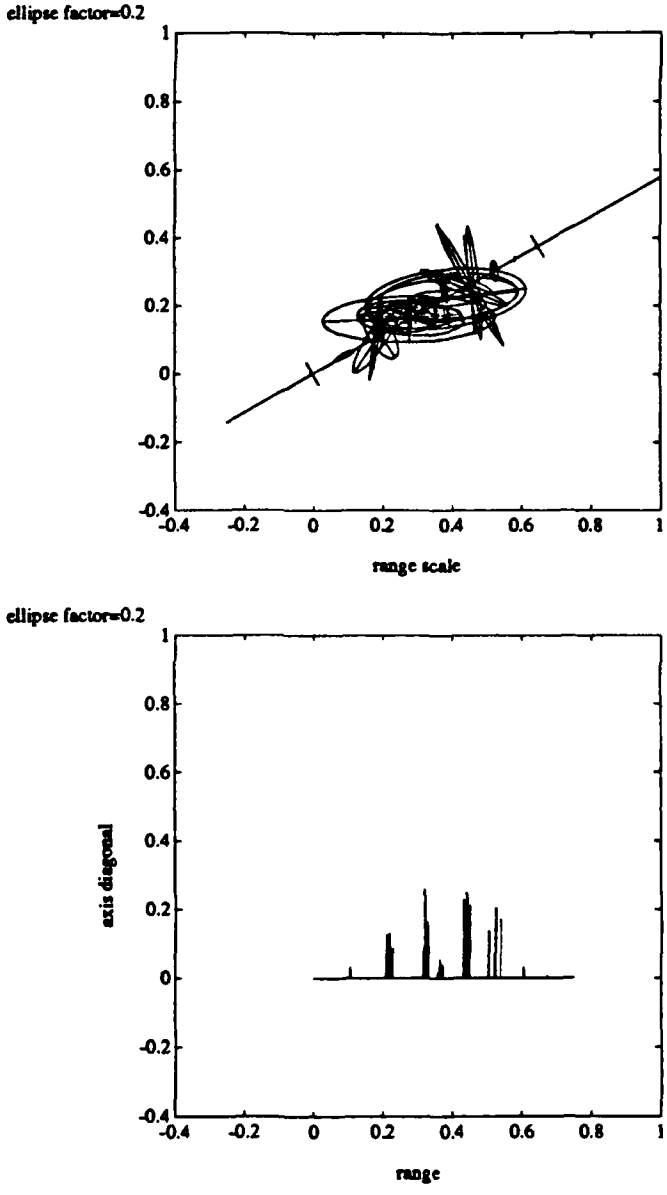

Figure 4.23: 707 Scatterers and Polarizations, SNR of 0dB

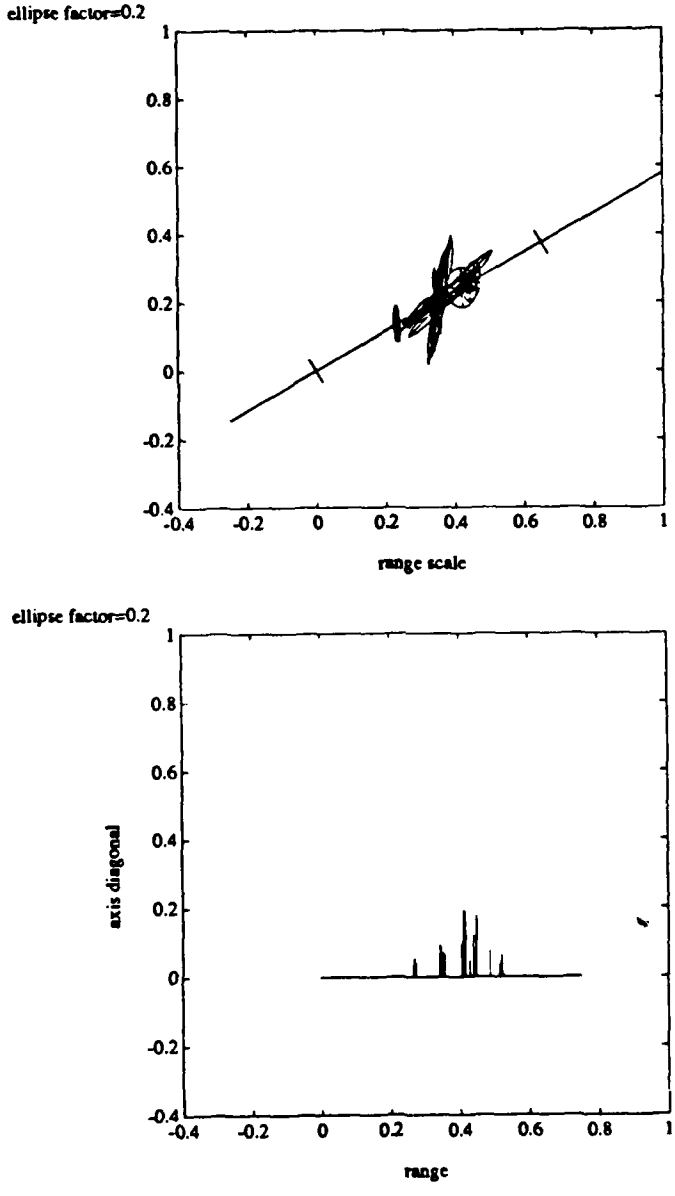

Figure 4.24: 727 Scatterers and Polarizations, SNR of 10dB

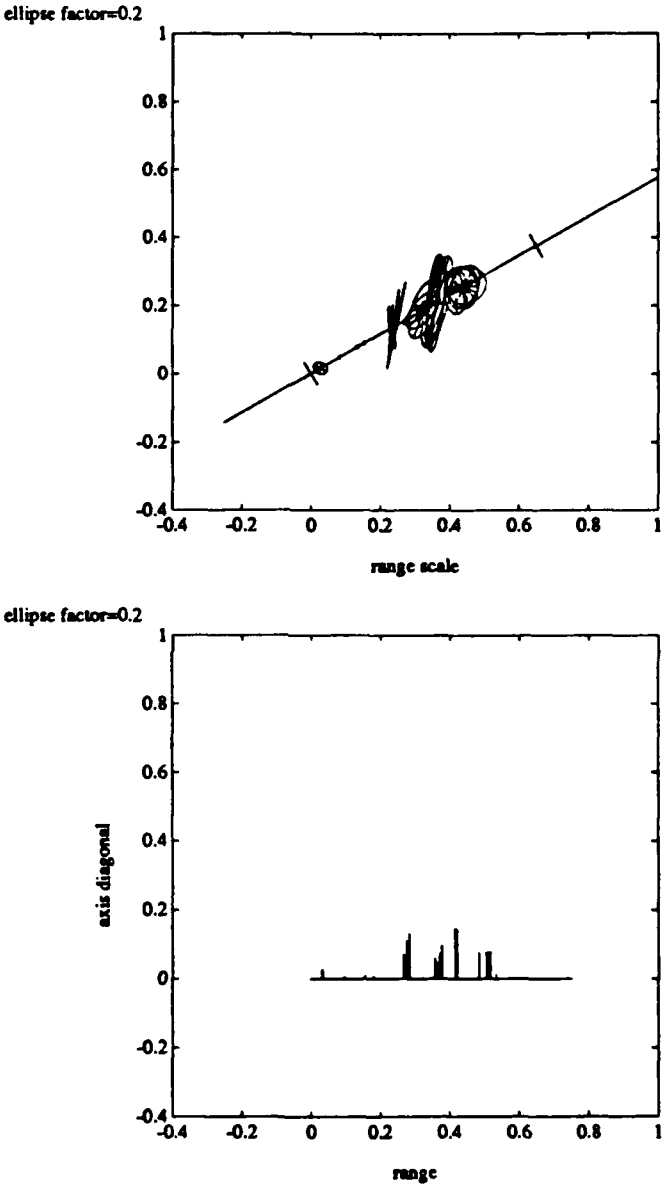

Figure 4.25: 727 Scatterers and Polarizations, SNR of 5dB

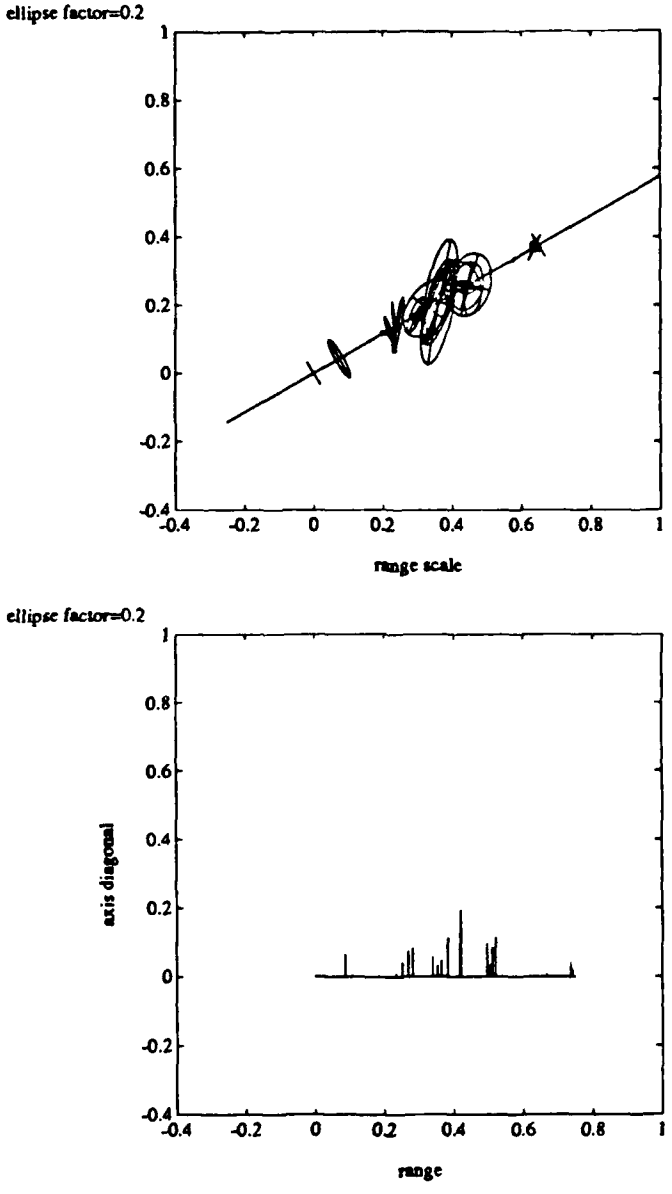

Figure 4.26: 727 Scatterers and Polarizations, SNR of 0dB

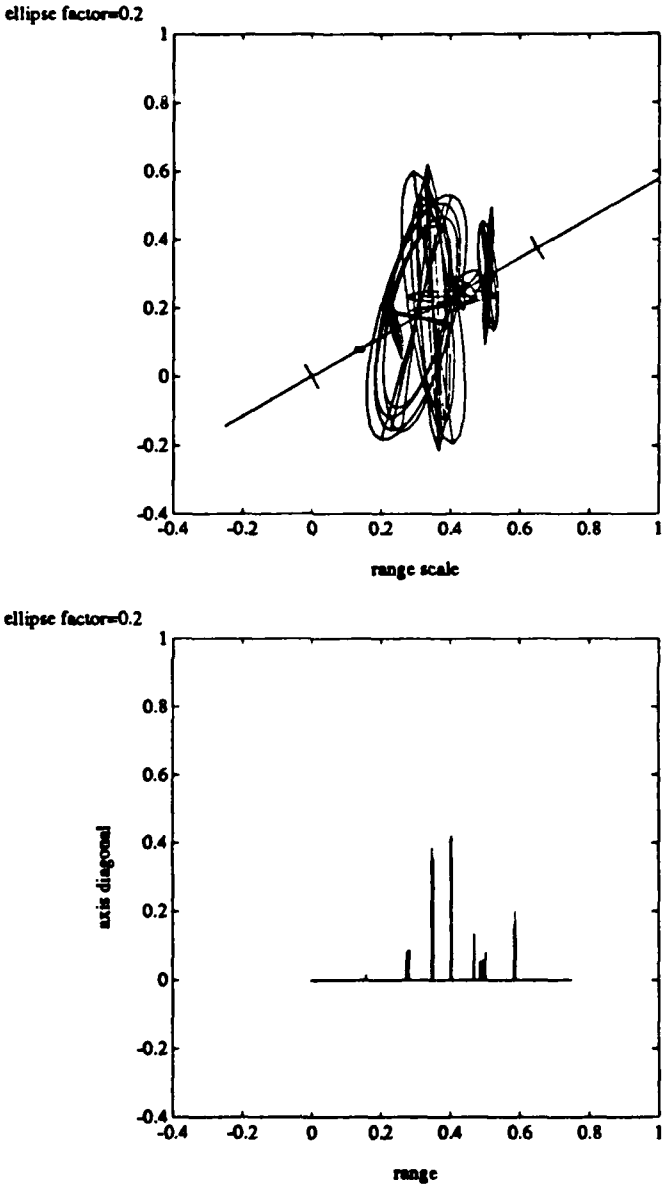

Figure 4.27: 747 Scatterers and Polarizations, SNR of 10dB

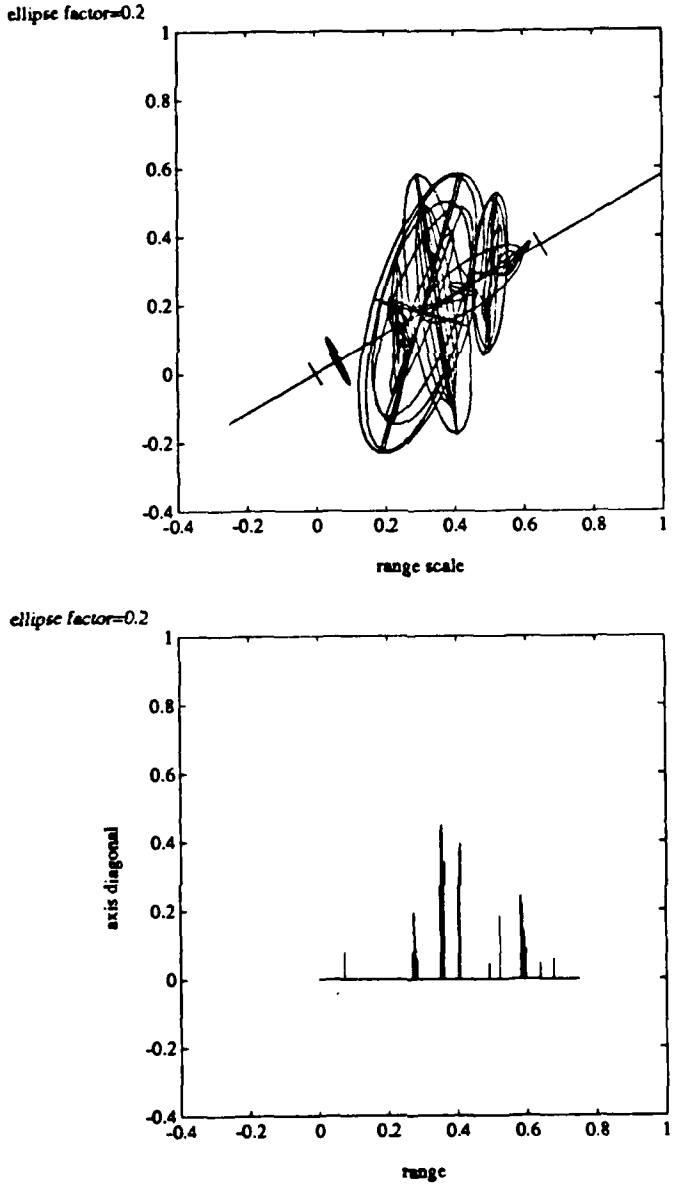

Figure 4.28: 747 Scatterers and Polarizations, SNR of 5dB

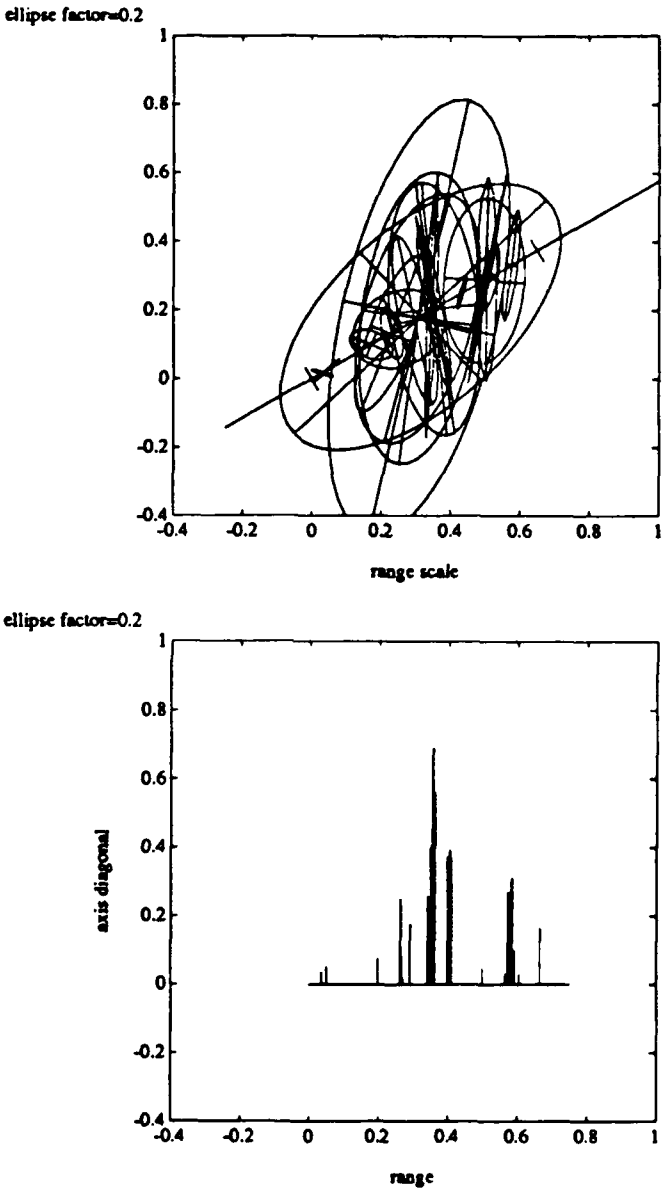

Figure 4.29: 747 Scatterers and Polarizations, SNR of 0dB

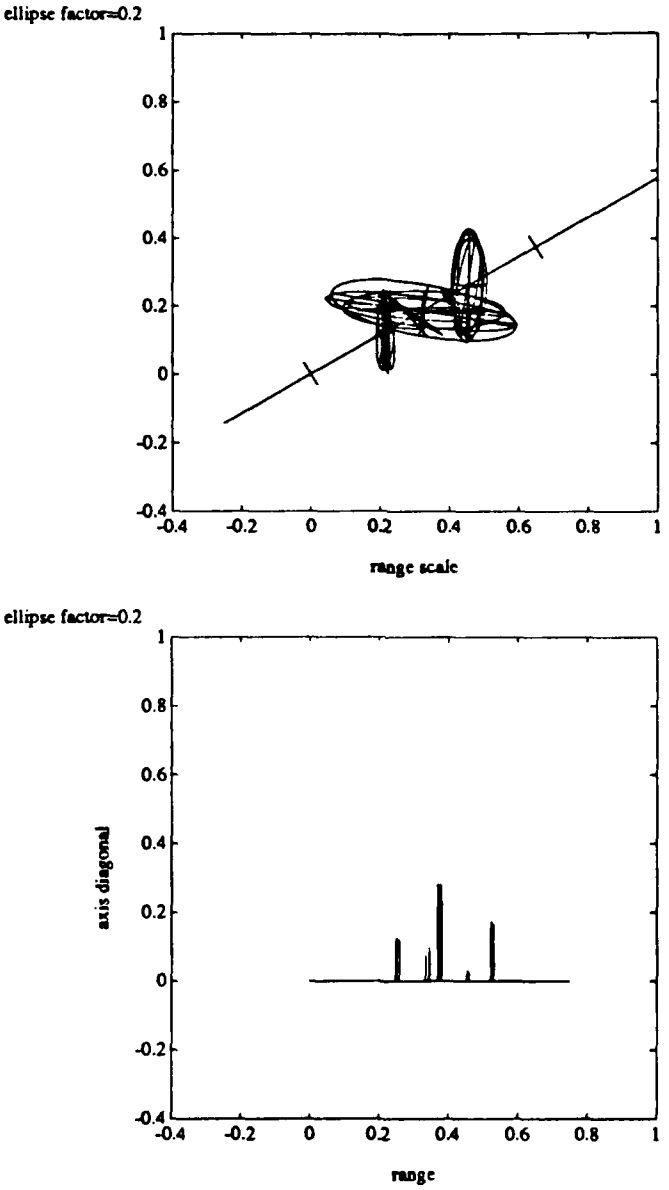

Figure 4.30: DC10 Scatterers and Polarizations, SNR of 10dB

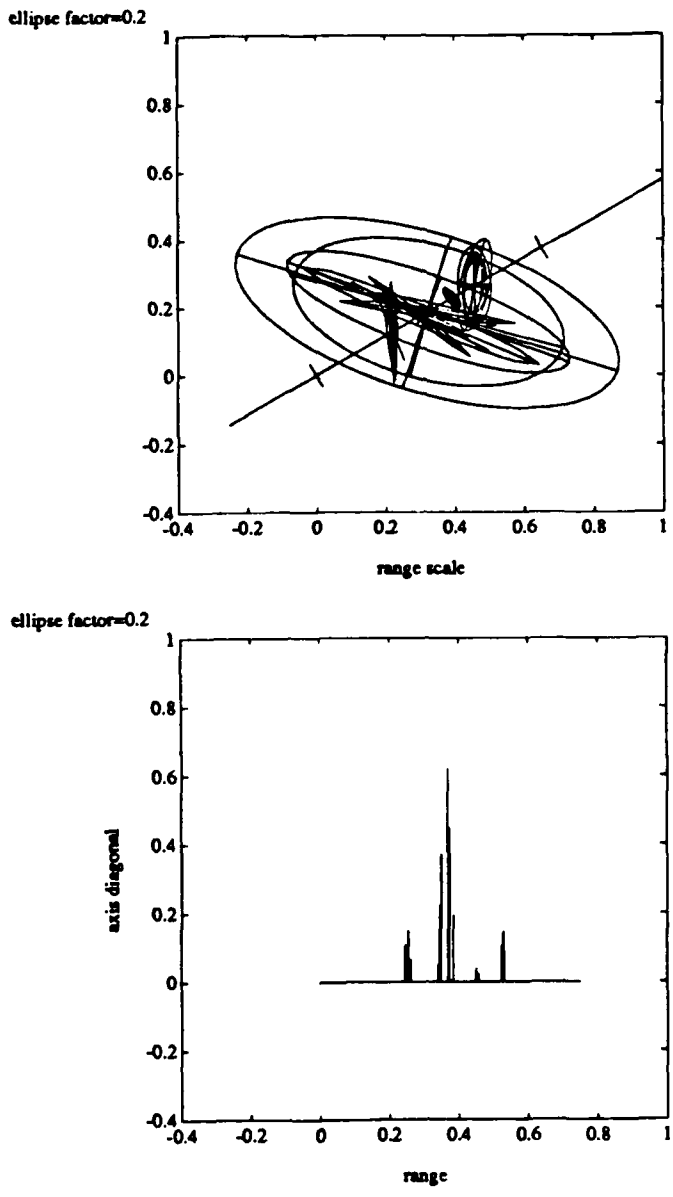

Figure 4.31: DC10 Scatterers and Polarizations, SNR of 5dB

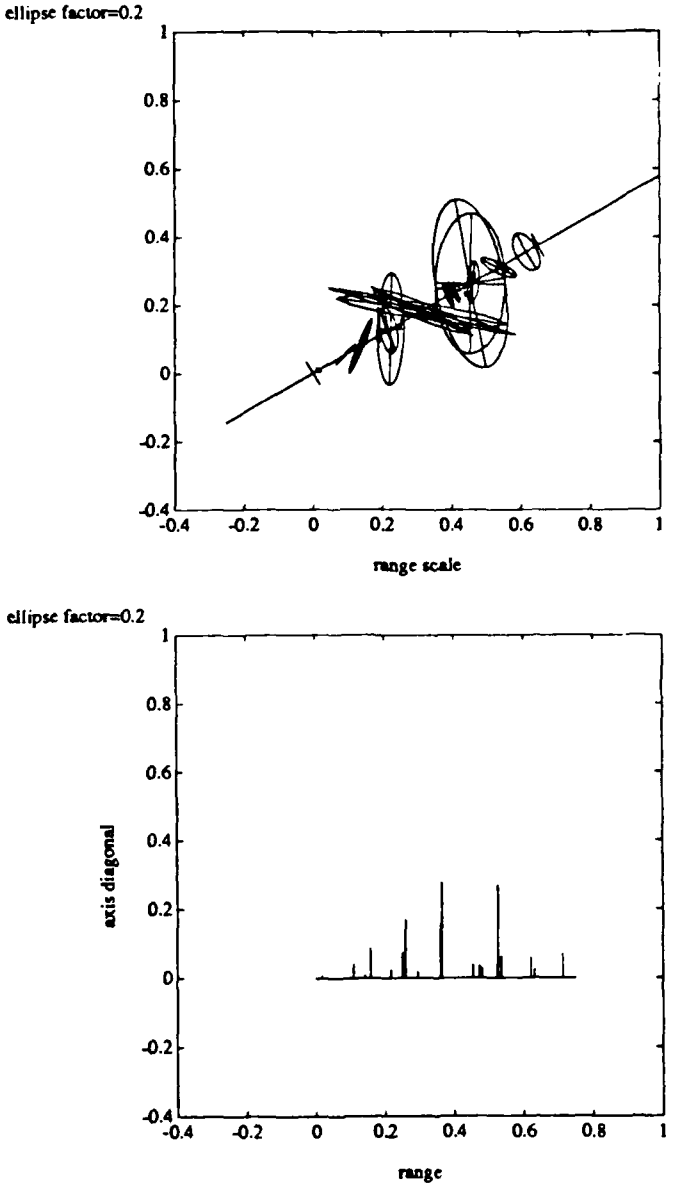

Figure 4.32: DC10 Scatterers and Polarizations, SNR of 0dB

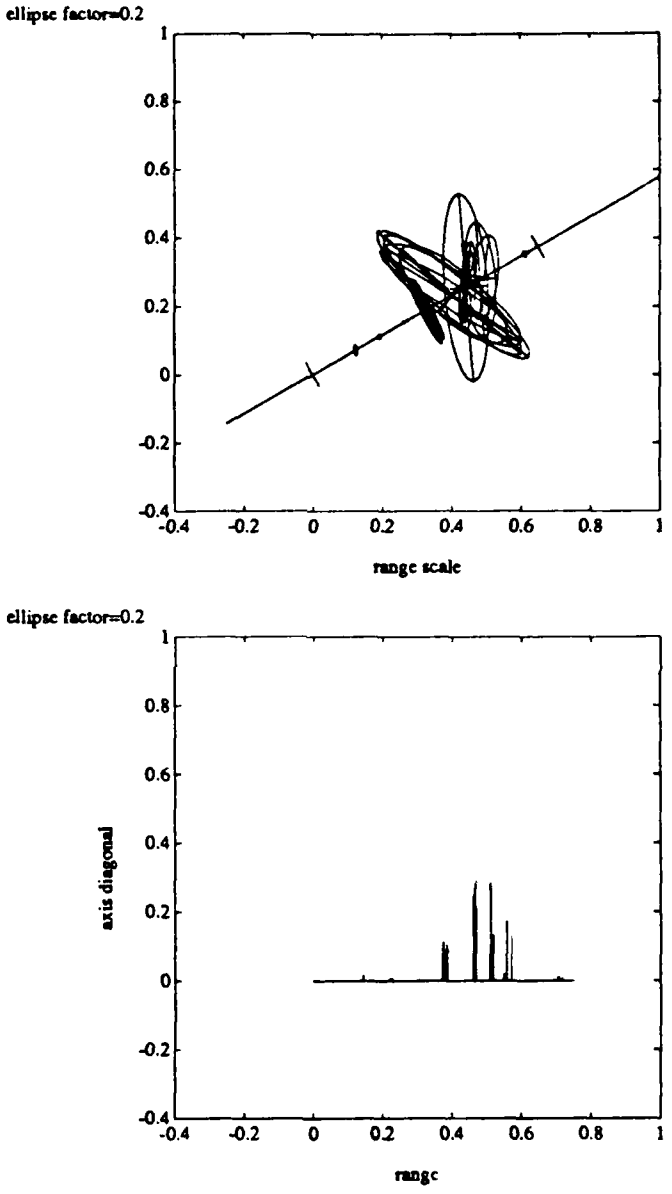

Figure 4.33: Concord Scatterers and Polarizations, SNR of 10dB

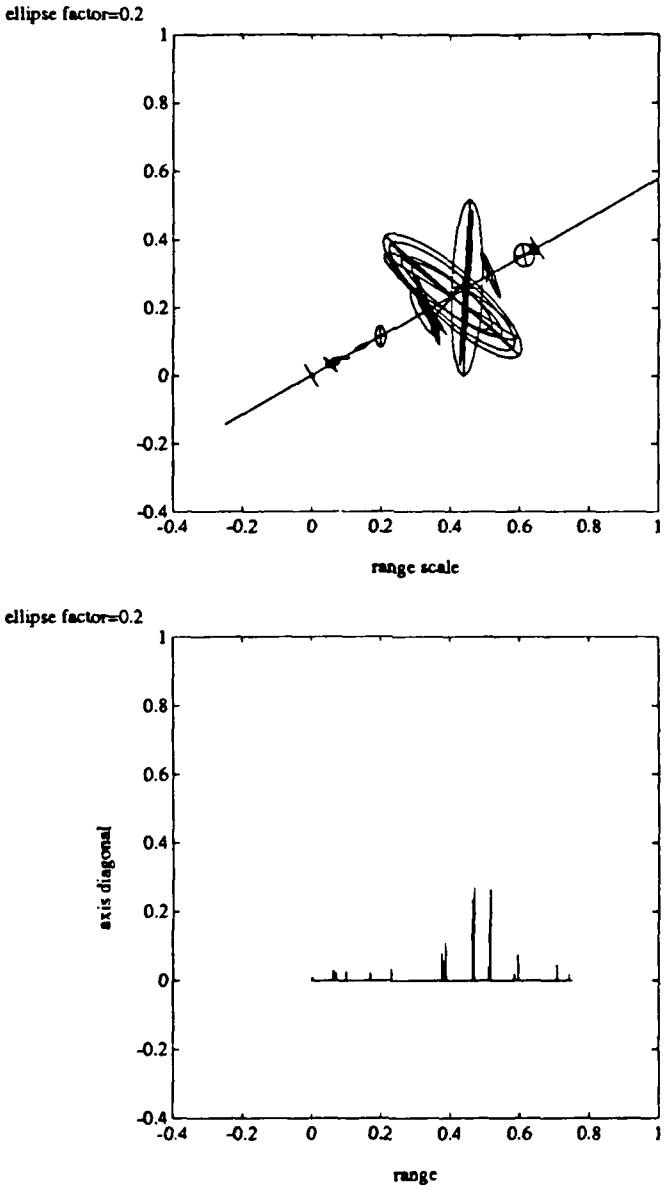

Figure 4.34: Concord Scatterers and Polarizations, SNR of 5dB

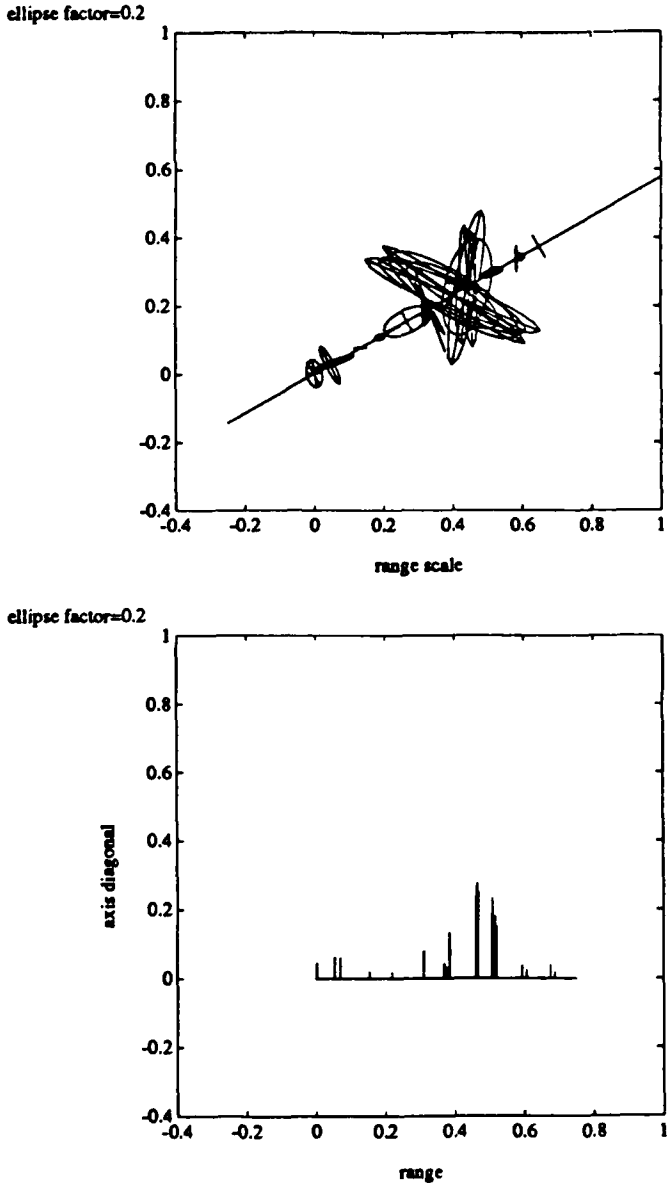

Figure 4.35: Concord Scatterers and Polarizations, SNR of 0dB

4.4 Summary of Simulation Results

The simulation results demonstrate that this estimation procedure produces target signatures which are unique, identifiable, and appropriate representations of the target. They also show that it still provides good results in the presence of noise, particularly in finding the range of a scatterer. This is due to the fact that both sets of data, $s_{hl}(f)$ and $s_{vl}(f)$, are used to determine the poles of the model. Even at 0 dB SNR the scattering centers are quite distinguishable, particularly in the hypotenuse plots. The polarization ellipse for each scatterer, however, is not as robust since its components are each derived from half of the data separately. Still, the scatterer center location may make identification of the target possible in these high noise situations. The scatterers also appear at down range locations which correspond with features of the planes such as wings, engine inlets, etc., which gives physical significance to the model and helps to motivate its use.

Chapter 5

Conclusions

This report has presented a method of processing full polarization, stepped frequency measurements of a target. The target is modeled based on the Transient Polarization Response concept introduced in [8]. A parametric model which describes the target as a set of scattering centers is developed. Each scattering center is characterized by a polarization ellipse, which corresponds to the backscattered polarization ellipse from a circularly polarized incident wave. An estimation procedure which directly estimates the parameters of this model is then developed. Simulation results are presented for both synthetic data and compact range measurements of aircraft. Results of this algorithm applied to these data verify that it is capable of identifying scattering mechanisms of the target, and that the estimated polarization ellipse of each scattering center correlates well with the geometry of the target. The signatures of various aircraft are seen to show such features as wings, engine inlets, cockpit cavity, and tail. Tests using noisy data shows that dominant scattering is well estimated even at 0 dB SNR.

5.1 Future Work

Although this procedure has provided promising initial results, more research needs to be done. A better understanding of how scattering centers interact with incident waves would be helpful in providing a mathematical analysis of the various scattering centers which appear in the model estimates. This would involve an understanding of the electromagnetic theory behind the scattering mechanisms. The robustness of the algorithm with respect to small changes in aspect angle also needs to be examined so that when a target's aspect is known only to within a certain degree and there are a finite number of aspects in the catalog a proper comparison can still be made. This obviously brings up the point that an effective way of comparing a target's model estimate to a catalog needs to be found so that it can be properly identified, which is, of course, the end goal. The model order and number of singular values to be kept are also areas for future research. Their determination needs to be automated in some way.

Bibliography

[1] A.A. Ksienski, Y.T. Lin, and L.J. White, "Low-frequency Approach to Target Identification," *Proceedings of the IEEE*, Vol. 63, No. 12, pp. 1651–1660, December 1975.

[2] D.L. Mensa, *High Resolution Radar Imaging*. Dedham, MA: Artech House, 1981.

[3] A. Kamis, F.D. Garber, and E.K. Walton, "Radar Target Classification Studies—Software Development and Documentation," Technical Report 716559-1, The Ohio State University, Department of Electrical Engineering, ElectroScience Laboratory, September 1985.

[4] J.S. Chen and E.K. Walton, "Comparison of Two Target Classification Techniques," *IEEE Transactions on Aerospace and Electronic Systems*, Vol. AES-22, No. 1, pp. 15–22, 1986.

[5] T.T. Goh, E.K. Walton, and F.D. Garber, "X-band ISAR Techniques for Radar Target Identification," Technical Report 717975-1, The Ohio State University, Department of Electrical Engineering, ElectroScience Laboratory, March 1987.

[6] R.L. Moses and J. Carl, "Autoregressive Modeling of Radar Data with Application to Target Identification," in *Proceedings of the IEEE 1988 National Radar Conference*, pp. 220–224, Ann Arbor, MI, April 20–21, 1988.

[7] R. Carrière and R.L. Moses, "Autoregressive Moving Average Modeling of Radar Target Signatures," in *Proceedings of the IEEE 1988 National Radar Conference*, pp. 225–229, Ann Arbor, MI, April 20–21, 1988.

[8] N.F. Chamberlain, "Recognition and Analysis of Aircraft Targets by Radar, Using Structural Pattern Representations Derived from Polarimetric Signatures," Ph.D. Dissertation, The Ohio State University, June 1989. Also: ElectroScience Laboratory Report 719710-3.

[9] N.F. Chamberlain, E.K. Walton, and F.D. Garber, "Radar Target Identification of Aircraft Using Polarization-diverse Features," *IEEE Transactions on Aerospace and Electronic Systems*, 1989. (in review).

[10] J.D. Kraus and K.R. Carver, *Electromagnetics*. New York, NY: McGraw-Hill, 1973.

[11] S.M. Kay, *Modern Spectral Estimation, Theory and Application*. Englewood Cliffs, NJ: Prentice-Hall, 1988.

[12] L. Marple, *Digital Spectral Analysis with Applications*. Englewood Cliffs, NJ: Prentice-Hall, 1987.

[13] R. Kumaresan and D.W. Tufts, "Estimating the Parameters of Exponentially Damped Sinusoids and Pole-zero Modeling in Noise," *IEEE Transactions on Acoustics, Speech, and Signal Processing*, Vol. ASSP-30, No. 6, pp. 833 840, December 1982.